# REPORT 1280

## THEORETICAL INVESTIGATION OF FLUTTER OF TWO-DIMENSIONAL FLAT PANELS WITH ONE SURFACE EXPOSED TO SUPERSONIC POTENTIAL FLOW [1]

By Herbert C. Nelson and Herbert J. Cunningham


### SUMMARY

*A Rayleigh type analysis involving chosen modes of the panel as degrees of freedom is used to treat the flutter of a two-dimensional flat panel supported at its leading and trailing edges and subjected to a middle-plane tensile force. The panel has a supersonic stream passing over its upper surface and still air below. The aerodynamic forces due to the supersonic stream are obtained from the theory for linearized two-dimensional unsteady flow and the forces due to the still air are obtained from acoustical theory.*

*In order to study the effect of increasing the number of modes in the analysis, two and then four modes are employed. The modes used are the first four natural modes of the panel in a vacuum with no tensile force acting. The analysis includes these variables: Mach number, structural damping, tensile force, density of the still air, and edge fixity (clamped and pinned). For certain combinations of these variables, stability boundaries are obtained which can be used to determine the panel thickness required to prevent flutter for any panel material and altitude.*

*In contrast to some previous panel-flutter investigations, the results of the present analysis show that sufficiently thick panels are flutter free for the Mach numbers treated and suggest that this is true throughout the supersonic speed range.*

*A comparison of results from the present theory for flat panels and from a criterion developed by R. P. Isaacs for the static stability of buckled panels is made with a few experimental results on flat and buckled panels clamped at leading and trailing edges.*


### INTRODUCTION

The flutter of thin metal plates or panels, such as compose the covering or skin of missiles and other craft intended for high-speed flight, has recently become of increased concern. Such panels may be initially flat or curved and may be small or fairly large in aspect ratio. In addition, they may be prestressed and will probably become warped in flight by aerodynamic heating. If one or more of the panels on a particular configuration are vibrating, the basic structure supporting them can usually be considered rigid. The fixity at the edges of the panels ranges between clamped and pinned, depending on the construction. Some preliminary experimentation and analytical work suggests that this type of instability is of concern only at supersonic speeds.

The problem of panel flutter embraces so many possible factors as to discourage general treatment, and previous papers on the subject (for example, refs. 1 to 7) have employed various simplifying assumptions in order to obtain specific solutions to what might perhaps be considered different phases of the problem. In all the references cited, the main assumption made is that a panel and the flow over it are two-dimensional. Other assumptions common to the reference papers are that small-deflection plate theory and linearized flow theory may be used.

References 1 to 4 examine the case of a panel buckled by a constant shortening and held at its leading and trailing edges, with a supersonic stream over its upper surface and no perturbation pressures on its lower surface. In reference 1 steady-state air forces and in reference 2 quasi-stationary air forces, which include the first order of the frequency of oscillation, are used. Both these references consider the dynamic stability of the buckled panel. Reference 3 and the more exhaustive reference 4 examine the static stability of the buckled panel and propose that motion (flutter) is the result when static equilibrium is not possible. Reference 5 and a section of reference 2 treat the case of a flat panel pinned at its leading and trailing edges. Reference 5 uses exact linearized unsteady aerodynamic forces and therefore, in contrast to reference 2, imposes no limitations on the order of the frequency. In references 1, 2, and 5 a generalized-coordinate approach involving chosen modes of the panel as degrees of freedom is employed. Reference 6, on the other hand, indicates how the problem of a vibrating membrane in a supersonic stream can be treated by means of Laplace transforms and suggests that similar treatment can be given to the plate problem. Reference 7 treats the case of a two-dimensional panel on many equally spaced simple supports with compressible air flowing over the upper surface and dead air below the panel, and the results indicate that the possible panel instabilities are divergence for subsonic flow and flutter for supersonic flow. Some questionable features of the results obtained in references 2, 5, and 7 are examined in the section entitled "Results and Discussion" in the present report.

A Rayleigh type flutter analysis is developed herein by means of Galerkin's process for a two-dimensional flat panel held in some manner at its leading and trailing edges and acted on by a middle-plane or axial force (which, in the case of tension, introduces a restoring force similar to that for the membrane). The upper surface of the panel is subjected to

[1] Supersedes NACA Technical Note 3465 by Herbert C. Nelson and Herbert J. Cunningham, 1955.

a supersonic stream and the lower surface to an unconfined mass of stationary compressible air. The normal modes of the panel with no middle-plane force acting are used as degrees of freedom in the analysis. As in reference 5, exact linearized unsteady aerodynamic forces are employed. In the reference paper the integrals yielding these forces are evaluated analytically. In the present report these integrals are evaluated numerically.

Numerical results are presented in order to examine some effects of including two and then four modes in the analysis and to determine effects of Mach number, density of the supersonic stream, panel mass and stiffness, edge fixity (to some extent), structural damping, axial load, and density of the still air below the panel. In appendix A an alternative solution by means of Laplace transforms is developed for the plate problem just described. No numerical results are obtained by this method, however.

A comparison of results from the theory presented herein for flat panels and from a criterion of reference 3 for the static stability of buckled panels is made with a few experimental results for flat and buckled panels clamped at the leading and trailing edges.

## SYMBOLS

| | |
|---|---|
| $a$ | speed of sound in undisturbed medium |
| $A_{mn},B_{mn},C_{mn}$ | structural and aerodynamic integrals defined after equation (13) |
| $c$ | panel chord |
| $D$ | local flexural stiffness, $\frac{E\tau^3}{12(1-\nu^2)}$ |
| $E$ | Young's modulus of elasticity of panel material |
| $f$ | tension parameter, $F/c^2m_A\omega_1^2$ |
| $f_\lambda$ | functions defined in equation (24) |
| $F$ | external force per unit width acting in midplane of panel (tensile force positive) |
| $g$ | structural damping coefficient |
| $G_{mn}$ | matrix elements defined in equation (13) |
| $H_0^{(2)}(u)$ | Hankel function of second kind, of zero order, (notation of ref. 18) |
| $I_{mn},\overline{I}_{mn},\overline{\overline{I}}_{mn}$ | aerodynamic integrals defined after equation (23) |
| $J_p(u),Y_p(u)$ | Bessel functions of order $p$ of first and second kind, respectively, (notation of ref. 18) |
| $k$ | reduced frequency, $c\omega/2U$ |
| $k_1$ | stiffness parameter (reduced first natural frequency), $c\omega_1/2U$ |
| $K_n$ | eigenvalues defined after equations (16) and (17) and given for first four panel modes in table I |
| $L(u),\overline{L}(u)$ | aerodynamic functions defined after equation (21) |
| $\overline{\overline{L}}_r(u)$ | aerodynamic functions defined after equation (B16) |
| $m_A$ | panel mass per unit surface area, $\sigma\tau$ |
| $M$ | Mach number, $U/a$ |
| $N_1,N_2$ | coefficients in mode-shape equations (16) and (17), given for first four panel modes in table I |
| $p(x,t)$ | net perturbation pressure, positive downward |
| $p_n(x)$ | pressure coefficient associated with mode shape $Z_n$, defined in equation (20) |
| $p_u,p_l$ | upper- and lower-surface contributions to perturbation pressure, respectively |
| $p_\infty,p_0$ | pressures in undisturbed supersonic stream and still-air region, respectively |
| $P_n(x),\overline{P}_n(x),\overline{\overline{P}}_n(x)$ | components of $p_n(x)$ defined after equation (22) |
| $q$ | dynamic pressure, $\frac{1}{2}\rho U^2$ |
| $s_r$ | coefficients of equations (28) and (B15) tabulated in appendix B for first four modes of panel with clamped edges |
| $t$ | time |
| $U$ | velocity of supersonic stream |
| $x,y,z$ | coordinates defined in figure 1 |
| $z(x,t)$ | vertical displacement of panel |
| $Z(x)$ | flutter mode shape |
| $Z_n(x)$ | $n$th natural mode shape for panel vibrating in vacuo |
| $\mu$ | panel-air mass ratio, $m_A/\rho c$ |
| $\nu$ | Poisson's ratio |
| $\rho,\rho_0$ | densities in undisturbed supersonic stream and still-air region, respectively |
| $\sigma$ | density of panel material |
| $\tau$ | local thickness of panel |
| $\phi$ | disturbance-velocity potential |
| $\omega$ | frequency of oscillation |
| $\omega_n$ | frequency associated with mode shape $Z_n$ |
| $\bar{\omega}$ | frequency parameter, $2kM^2/\beta^2$ |
| $\Omega$ | frequency ratio squared $\left(\frac{\omega_1}{\omega}\right)^2$, except in flutter calculations where $\Omega=\left(\frac{\omega_1}{\omega}\right)^2(1+ig)$ |
| [ ] | square matrix |
| { } | column matrix |

Subscripts:

| | |
|---|---|
| $u$ | upper-surface contribution |
| $l$ | lower-surface contribution |

Primes denote differentiation with respect to the argument.

## ANALYSIS

### STATEMENT OF PROBLEM

A thin isotropic, two-dimensional plate (beam) of constant thickness, as shown in figure 1, is considered herein. The plate is undergoing simple harmonic motion and is acted on by a middle-plane or axial force $F$ (tension or compression); its upper surface is subjected to a supersonic stream of velocity $U$, pressure $p_\infty$, and density $\rho$, and its

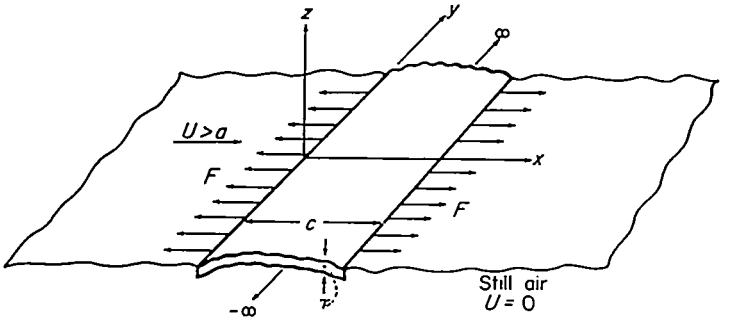


FIGURE 1.—Sketch of flexible two-dimensional panel.

lower surface is subjected to still air with pressure $p_0$ and density $\rho_0$. The differential equation of motion for the plate may be written as

$$D\frac{\partial^4 z}{\partial x^4}+m_A\frac{\partial^2 z}{\partial t^2}-F\frac{\partial^2 z}{\partial x^2}+(p_\infty-p_0)+p(x,t)=0 \qquad (1)$$

where, in the present case, the vertical displacement of the plate $z(x,t)$ may be expressed as $Z(x)e^{i\omega t}$, $\omega$ is the circular frequency of oscillation, $p(x,t)$ is the net perturbation pressure (positive downward) arising from the motion of the plate, $m_A$ is the plate mass per unit surface area, and the local flexural stiffness $D$ is given by $E\tau^3/12(1-\nu^2)$. For the case where $p(x,t)=0$, equation (1) may be obtained, with appropriate changes in notation, from reference 8.

In the remaining development the constant-pressure term $p_\infty-p_0$ of equation (1) is considered to be zero. This in no way affects the generality of the results for the oscillating plate, since inclusion of the constant-pressure term as nonzero would result only in adding a particular solution which represents a static vertical deflection. In addition, the coordinate $x$ of equation (1) is divided by the plate chord $c$ and henceforth is employed in this nondimensional sense. Thus, equation (1) multiplied by $e^{-i\omega t}$ becomes

$$\frac{D}{c^4}Z''''-\omega^2 m_A Z-\frac{F}{c^2}Z''+p(x,t)e^{-i\omega t}=0 \qquad (2)$$

where the primes denote differentiation with respect to the argument $x$.

In order to obtain a specific solution of equation (2), four boundary conditions are required. The plate is considered to be held at its leading and trailing edges as shown in figure 1, and this assumption leads to the conditions for pinned edges:

$$Z(0)=Z(1)=Z''(0)=Z''(1)=0 \qquad (3)$$

and for clamped edges:

$$Z(0)=Z(1)=Z'(0)=Z'(1)=0 \qquad (4)$$

In a later section of the analysis the boundary-value problems, as exemplified by equations (2) and (3) or (2) and (4), are solved by Galerkin's method. Also considered in appendix A are the solutions to these problems by means of Laplace transforms.

### NET PERTURBATION PRESSURE $p(x,t)$

The net pressure $p(x,t)$, as mentioned previously, arises from the oscillatory motion of the plate. It is this pressure which damps, or in the case of flutter sustains, the oscillation. The pressure on the upper surface is obtained from the theory for linearized unsteady supersonic flow and the pressure on the lower surface from acoustical theory. The perturbation pressure in terms of the pressures $p_u$ on the upper surface and $p_l$ on the lower surface is

$$p(x,t)=p_u-p_l \qquad (5)$$

where

$$p_u=\rho\left(\frac{\partial\phi_u}{\partial t}+\frac{U}{c}\frac{\partial\phi_u}{\partial x}\right) \qquad (6)$$

and

$$p_l=\rho_0\frac{\partial\phi_l}{\partial t} \qquad (7)$$

From reference 9 the velocity potential for the upper surface can be obtained in the form

$$\phi_u=\frac{ce^{i\omega t}}{\beta}\int_0^x\left[i\omega Z(\xi)+\frac{U}{c}\frac{dZ}{d\xi}\right]e^{-i\bar{\omega}(x-\xi)}J_0\left[\frac{\bar{\omega}}{M}(x-\xi)\right]d\xi \qquad (8)$$

where

$$\bar{\omega}=\frac{2kM^2}{\beta^2} \qquad \beta=\sqrt{M^2-1} \qquad k=\frac{\omega c}{2U}$$

Based on reference 10, the velocity potential for the lower surface can be obtained, as shown in appendix B, in the form

$$\phi_l=-\frac{\omega ce^{i\omega t}}{2}\int_0^1 Z(\xi)H_0^{(2)}(2kM|x-\xi|)d\xi \qquad (9)$$

where $H_0^{(2)}(x)$ is the Hankel function of the second kind, of zero order.

### SOLUTION BY GALERKIN'S METHOD

Outline of method.—The boundary-value problems considered earlier (eqs. (2) and (3) for the pinned-edge plate and equations (2) and (4) for the clamped-edge plate) are now solved by means of Galerkin's method. (A detailed account of Galerkin's method may be found in ref. 11.) As a first step, the flutter mode shape $Z(x)$ is approximated by a linear combination of the form

$$Z(x)=c\sum_{n=1}^{N}a_n Z_n(x) \qquad (10)$$

where the coefficients $a_n$ may represent complex amplitudes and where the functions $Z_n(x)$ are the mode shapes for the plate vibrating in a vacuum without an axial force $F$ acting. The function $Z_1$ is the fundamental mode shape associated with the lowest natural frequency $\omega_1$, and the remaining functions $Z_2, Z_3, \ldots Z_N$ are consecutively the higher modes

shapes. The shapes $Z_n$ satisfy the pinned-edge or clamped-edge boundary conditions ($Z_n$ replacing $Z$ in eqs. (3) and (4)) and the differential equation

$$\frac{D}{c^4} Z_n'''' - \omega_n^2 m_A Z_n = 0 \tag{11}$$

where $\omega_n$ is the frequency of oscillation for which $Z_n$ is the mode shape.

The remainder of the Galerkin process for solving the aforementioned boundary-value problems consists of determining the coefficients $a_n$ of equation (10) in the following manner: Substitute equation (10) into equation (2), replace the term $\frac{D}{c^4} Z_n''''$ by $\omega_n^2 m_A Z_n$ in accordance with equation (11), multiply by one of the mode shapes $Z_m$, integrate the result from $x=0$ to $x=1$, and equate to zero. When $n$ is made 1, 2, . . . $N$ in succession, $N$ linear equations are obtained which determine the unknowns $a_n$. These equations can be written in the form

$$\begin{bmatrix} G_{11} & G_{12} & \dots & G_{1N} \\ G_{21} & G_{22} & \dots & G_{2N} \\ \cdot & \cdot & \dots & \cdot \\ G_{N1} & G_{N2} & \dots & G_{NN} \end{bmatrix} \begin{Bmatrix} a_1 \\ a_2 \\ \cdot \\ a_N \end{Bmatrix} = \begin{Bmatrix} 0 \\ 0 \\ \cdot \\ 0 \end{Bmatrix} \tag{12}$$

The matrix elements are given by

$$G_{mn} = \mu \left\{ A_{mn} - \Omega \left[ \left( \frac{\omega_m}{\omega_1} \right)^2 A_{mn} + f B_{mn} \right] \right\} - C_{mn} \tag{13}$$

where

$$\mu = \frac{m_A}{\rho c} \qquad A_{mn} = \int_0^1 Z_m Z_n \, dx$$

$$\Omega = \left( \frac{\omega_1}{\omega} \right)^2 \qquad B_{mn} = \int_0^1 Z_m' Z_n' \, dx$$

$$f = \frac{F}{c^2 m_A \omega_1^2} \qquad C_{mn} = \int_0^1 Z_m p_n(x) dx$$

and where $p_n(x)$ is the pressure $p(x,t)$, obtained from equations (5) to (9) with $Z$ replaced by $Z_n$, multiplied by $e^{-i\omega t}/\rho c \omega^2$. In equation (13) $\omega_1$ and $\omega_n$ are the first and the $m$th natural frequency, respectively, of the plate with no axial force acting.

**Flutter determinant.**—The flutter condition or condition of harmonic vibration, which is given by the nontrivial solution for the coefficients $a_n$, is obtained from equation (12) by setting the determinant of the matrix $G_{mn}$ equal to zero. Thus the flutter condition may be expressed in the form

$$\begin{vmatrix} G_{11} & G_{12} & \dots & G_{1N} \\ G_{21} & G_{22} & \dots & G_{2N} \\ \cdot & \cdot & \dots & \cdot \\ G_{N1} & G_{N2} & \dots & G_{NN} \end{vmatrix} = 0 \tag{14}$$

**Remarks on alternative procedure.**—The procedure from equation (11) to equation (13) is, in general, not the most accurate that could be followed for values of $F$ other than zero. A generally more accurate procedure would be to use, instead of equation (11), the differential equation for the panel with tension:

$$\frac{D}{c^4} Z_n'''' - \omega_n^2 m_A Z_n - \frac{F}{c^2} Z_n'' = 0 \tag{15}$$

When equation (15) is solved, subject to the appropriate boundary conditions, the frequencies $\omega_n$ are found to be functions of $F$ for both pinned and clamped edges, but the mode shapes $Z_n$ do not vary with $F$ for pinned edges. The use of equation (15) rather than equation (11) would mean that in equation (13) the term $fB_{mn}$ would not appear and the frequencies and mode shapes would be those that satisfy equation (15).

Equation (11) rather than equation (15) has been used herein for the following reasons: For pinned-edge panels there is no difference in the mode shapes or in the final numerical flutter results; for clamped-edge panels the determination of the values of $Z_n$ and $\omega_n$ that satisfy equation (15) is laborious and must be carried out for every desired value of $F$. Elimination of the term $fB_{mn}$ from the matrix elements, through use of equation (15), does not compensate for the labor of determining the natural frequencies and mode shapes as functions of $F$. The differences in final numerical flutter results for the clamped-edge panel approach zero as the number of modes in the analysis is increased and are expected to be small even when only a few modes are used.

## EVALUATION OF TERMS IN FLUTTER DETERMINANT

**Structural integrals $A_{mn}$ and $B_{mn}$ and frequencies $\omega_n$.**—Consideration will now be given to the evaluation of the mode-shape integrals and frequencies in the elements of equation (15). The mode shapes $Z_n$ and associated natural frequencies $\omega_n$ obtained from equation (12) are:

For the pinned-edge plate,

$$\left.\begin{aligned} Z_n &= N_1 \sin K_n x \\ \omega_n &= K_n^2 \sqrt{\frac{D}{m_A c^4}} \end{aligned}\right\} \tag{16}$$

where $K_n$ is obtained from the frequency equation

$$\sin K_n=0$$

For the clamped-edge plate,

$$\left.\begin{aligned} Z_n&=N_1[\cos K_n x-\cosh K_n x+N_2(\sin K_n x-\sinh K_n x)] \\ \omega_n&=K_n^2\sqrt{\frac{D}{m_A c^4}} \end{aligned}\right\} \quad (17)$$

where $K_n$ is obtained from the frequency equation

$$\cos K_n \cosh K_n=1$$

In equations (16) and (17) the factor $N_1$ is used to produce unit deflection at the center of the plate ($x=0.5$) for modes that are symmetric about the center and at the point of maximum deflection between the leading edge ($x=0$) and the center of the plate for modes that are antisymmetric about the center. The factor $N_2$ in equation (17) is established by the boundary condition requiring zero deflection at $x=1$ and is expressed by

$$N_2=-\frac{\cos K_n-\cosh K_n}{\sin K_n-\sinh K_n} \quad (18)$$

The quantities $\omega_1$, $\omega_m/\omega_1$, $A_{mn}$, and $B_{mn}$ required in equation (14) can be determined directly from equations (16) or (17). First, however, values must be established for $N_1$ and $K_n$ in the case of the pinned-edge plate and for $N_1$, $N_2$, and $K_n$ in the case of the clamped-edge plate. Table I includes values of all these quantities for the first four modes of vibration.

The values for $A_{mn}$ shown in table I are zero when $m\neq n$ because of the orthogonality of the mode shapes $Z_n$ of equations (16) and (17). For the pinned-edge case the slopes.

TABLE I.—MODE-SHAPE FACTORS, EIGENVALUES, FREQUENCY RATIOS, AND STRUCTURAL INTEGRALS FOR FIRST FOUR NORMAL MODES

(a) Pinned-edge plate [a]

| Mode, $n$ | $N_1$ | $N_2$ | $K_n$ | $\omega_n/\omega_1$ | $A_{nn}$ | $B_{nn}$ |
|---|---|---|---|---|---|---|
| 1 | 1 | -------- | $\pi$ | 1 | 0.5 | $0.5\pi^2$ |
| 2 | 1 | -------- | $2\pi$ | 4 | .5 | $2.0\pi^2$ |
| 3 | 1 | -------- | $3\pi$ | 9 | .5 | $4.5\pi^2$ |
| 4 | 1 | -------- | $4\pi$ | 16 | .5 | $8.0\pi^2$ |

[a] $A_{mn}=B_{mn}=0$ $(m\neq n)$

(b) Clamped-edge plate [b, c]

| Mode, $n$ | $N_1$ | $N_2$ | $K_n$ | $\omega_n/\omega_1$ | $A_{nn}$ | $B_{nn}$ |
|---|---|---|---|---|---|---|
| 1 | −0.629699 | −0.98250 | 4.730 | 1 | 0.396 | 4.88 |
| 2 | −.66260 | −1.000778 | 7.853204625 | 2.7566 | .440 | 21.2 |
| 3 | .7109645 | −.99997 | 10.99560784 | 5.404 | .506 | 49.8 |
| 4 | −.66120074 | −1.00000145 | 14.13716549 | 8.933 | .432 | 76.4 |

[b] $A_{mn}=0$ $(m\neq n)$
$B_{13}=B_{31}=4.362$
$B_{24}=B_{42}=-8.360$
Other $B_{mn}=0$ $(m\neq n)$
[c] The significant figures shown were used to avoid small-difference errors in mode shapes

$Z_n'$ of the mode shapes are also orthogonal and, consequently, $B_{mn}$ is zero when $m\neq n$. For the clamped-edge case, even though the slopes $Z_n'$ are not orthogonal, the integrand of $B_{mn}$ is antisymmetric about $x=0.5$ when $m$ and $n$ are not both even or both odd and, consequently, $B_{mn}$ is zero when $m\neq n$ except for $B_{13}$, $B_{31}$, $B_{24}$, and $B_{42}$ (for the first four modes).

**Aerodynamic integrals $C_{mn}$.**—The remaining term in the elements of equation (14) that requires evaluation is the integral

$$C_{mn}=\int_0^1 Z_m p_n(x)dx \quad (19)$$

As mentioned previously, $p_n(x)$ is the pressure $p(x,t)$, obtained from equations (5) to (9) with $Z$ replaced by $Z_n$, multiplied by $e^{-i\omega t}/\rho c\omega^2$. The quantity $p_n(x)$ is therefore given by

$$\begin{aligned} p_n(x)=\frac{1}{\beta}\Bigg(&\int_0^x\left[-Z_n(\xi)+\frac{i}{2k}\frac{dZ_n}{d\xi}\right]e^{-i\bar{\omega}(x-\xi)}J_0\left[\frac{\bar{\omega}}{M}(x-\xi)\right]d\xi+ \\ &\frac{-i}{2k}\frac{d}{dx}\left\{\int_0^x\left[-Z_n(\xi)+\frac{i}{2k}\frac{dZ_n}{d\xi}\right]e^{-i\bar{\omega}(x-\xi)}J_0\left[\frac{\bar{\omega}}{M}(x-\xi)\right]d\xi\right\}\Bigg)_u+ \\ &\frac{\rho_0}{\rho}\left[\frac{i}{2}\int_0^1 Z_n(\xi)H_0^{(2)}(2kM|x-\xi|)d\xi\right]_l \end{aligned} \quad (20)$$

where the contributions from the upper and lower surfaces of the plate are designated by subscripts $u$ and $l$, respectively. Upon elimination of the derivatives in the integrands of the upper-surface contribution through integration by parts, performance of the indicated differentiation of the second integral, and extraction of the singularity at $\xi=x$ in the Hankel function of the lower-surface contribution, equation (20) may be written in the form

$$p_n(x)=\frac{1}{\beta}\left[\int_0^x Z_n(\xi)L(x-\xi)d\xi+\frac{i}{2k}\frac{M^2-2}{\beta^2}Z_n(x)+\frac{1}{4k^2}Z_n'(x)\right]_u+\frac{\rho_0}{\rho}\left[\int_0^1 Z_n(\xi)\bar{L}(x-\xi)d\xi+\frac{1}{\pi}\int_0^1 Z_n(\xi)\log_e(kM|x-\xi|)d\xi\right]_l \quad (21)$$

where

$$L(u)=\left[-\frac{M^2+2}{2\beta^4}J_0\left(\frac{\bar{\omega}}{M}u\right)+i\frac{2M}{\beta^4}J_1\left(\frac{\bar{\omega}}{M}u\right)+\frac{M^2}{2\beta^4}J_2\left(\frac{\bar{\omega}}{M}u\right)\right]e^{-i\bar{\omega}u}$$

$$\bar{L}(u)=\frac{i}{2}J_0(2kM|u|)+\frac{1}{2}Y_0(2kM|u|)-\frac{1}{\pi}\log_e(kM|u|)$$

$$\bar{L}(0)=\frac{\gamma}{\pi}+\frac{i}{2}\qquad \gamma=0.577216 \text{ (Euler's constant)}$$

The quantities $J_p$ and $Y_p$ are the Bessel functions of order $p$, of the first and second kind, respectively.

For convenience $p_n(x)$ is considered in three parts, namely,

$$p_n(x)=P_n(x)+\bar{P}_n(x)+\bar{\bar{P}}_n(x) \tag{22}$$

where

$$P_n(x)=\frac{1}{\beta}\left[\int_0^x Z_n(\xi)L(x-\xi)d\xi+\frac{i}{2k}\frac{M^2-2}{\beta^2}Z_n(x)+\frac{1}{4k^2}Z_n'(x)\right]$$

$$\bar{P}_n(x)=\frac{\rho_0}{\rho}\int_0^1 Z_n(\xi)\bar{L}(x-\xi)d\xi$$

$$\bar{\bar{P}}_n(x)=\frac{\rho_0}{\rho}\frac{1}{\pi}\int_0^1 Z_n(\xi)\log_e(kM|x-\xi|)d\xi$$

Hence, equation (19) may be put in the form

$$C_{mn}=I_{mn}+\bar{I}_{mn}+\bar{\bar{I}}_{mn} \tag{23}$$

where

$$I_{mn}=\int_0^1 Z_m P_n(x)dx$$

$$\bar{I}_{mn}=\int_0^1 Z_m P_n(x)dx$$

$$\bar{\bar{I}}_{mn}=\int_0^1 Z_m \bar{\bar{P}}_n(x)dx$$

The first integral $I_{mn}$ represents the effect of the supersonic stream passing over the upper surface of the plate; the other two integrals represent the effect of the still air below the plate.

Before further development of the method of the present report for determining $C_{mn}$, the aerodynamic treatments of references 1, 2, and 5, which deal with the pinned-edge plate, will be examined. These references consider only the effects of the supersonic stream, the air below the plate being treated, in essence, as massless; that is, $\rho_0/\rho$ is taken to be zero and the integrals $\bar{I}_{mn}$ and $\bar{\bar{I}}_{mn}$ are omitted. In references 1 and 2 the aerodynamic effects are accounted for as if the integral $I_{mn}$ has been expanded as a power series in the frequency of oscillation; reference 1 retains only the steady-state or zero-order frequency term and reference 2 adds the first-order frequency term. In reference 5, on the other hand, the integral $I_{mn}$ is evaluated exactly with regard to the frequency. This is possible because the modal functions $Z_n$ for the pinned-edge plate are sine waves (see eq. (16)) so that $I_{mn}$ can be obtained in terms of the functions (sometimes called Schwarz functions)

$$f_\lambda(a,b)=\frac{1}{b^{\lambda+1}}\int_0^b u^\lambda e^{-iu}J_0\left(\frac{u}{a}\right)du\qquad(\lambda=0,1) \tag{24}$$

where

$$a=\frac{M}{\bar{\omega}}b$$

and $b$ has the four values

$$b=\bar{\omega}+\left\{\begin{matrix}\pm m\\ \pm n\end{matrix}\right\}\pi$$

A similar result could be obtained for the clamped-edge plate by approximating the modal functions $Z_n$ (see eq. (17)) by a finite sine series

$$Z_n\approx\sum_{r=1}^{R}d_r\sin r\pi x$$

For either pinned or clamped edges, the arguments $a$ and $b$ of the Schwarz functions $f_\lambda$ would range from large positive to large negative values, particularly for the higher modes, and would thus require extensive tabulation of $f_0$ and $f_1$. The exact expression for the pressure term $p_n(x)$ is employed in the present report but, because the necessary tables of $f_0$ and $f_1$ are not available, for convenience, a numerical method of integration is used to evaluate $p_n(x)$ and the aerodynamic integrals $I_{mn}$, $\bar{I}_{mn}$, and $\bar{\bar{I}}_{mn}$ of equation (23).

The numerical method is based on the following integration rules for parabolic arcs:

$$\int_{x_1}^{x_2}y(x)dx=\frac{\Delta x}{12}[5y(x_1)+8y(x_2)-y(x_3)] \tag{25a}$$

$$\int_{x_2}^{x_3}y(x)dx=\frac{\Delta x}{12}[-y(x_1)+8y(x_2)+5y(x_3)] \tag{25b}$$

where $x_2=x_1+\Delta x$ and $x_3=x_2+\Delta x$. The range of integration in equation (19), $0\leqq x\leqq 1$, is, for convenience, divided into an even number of equal segments. From the standpoint of accuracy the number of segments needed depends on the number of nodes in the highest mode and on the value of

$\bar{\omega}$ for which $p_n(x)$ is evaluated. For the numerical applications of the present report, 10 segments were found to be adequate, and the method of integration is illustrated for this number of segments in the equations to follow.

The use of 10 segments would, in general, require the determination of $p_n(x)$ in equation (19) at 11 points on the plate. However, the integrand of $C_{mn}$ at $x=0$ and $x=1$ is zero since the mode shapes $Z_m$ are zero at these points, and therefore $p_n(x)$ need be evaluated at only the 9 interior points (equally spaced between $x=0$ and $x=1$). The values of the terms $P_n$, $\bar{P}_n$, and $\bar{\bar{P}}_n$ of equation (22) for these points may be arranged in matrix form as follows:

$$\begin{Bmatrix} P_n(.1) \\ P_n(.2) \\ P_n(.3) \\ P_n(.4) \\ P_n(.5) \\ P_n(.6) \\ P_n(.7) \\ P_n(.8) \\ P_n(.9) \end{Bmatrix} = \frac{1}{120\beta} \begin{bmatrix} 8L(0) & -L(-.1) & 0 & 0 & 0 & 0 & 0 & 0 & 0 \\ 13L(.1) & 7L(0) & -L(-.1) & 0 & 0 & 0 & 0 & 0 & 0 \\ 13L(.2) & 12L(.1) & 7L(0) & -L(-.1) & 0 & 0 & 0 & 0 & 0 \\ 13L(.3) & 12L(.2) & 12L(.1) & 7L(0) & -L(-.1) & 0 & 0 & 0 & 0 \\ 13L(.4) & 12L(.3) & 12L(.2) & 12L(.1) & 7L(0) & -L(-.1) & 0 & 0 & 0 \\ 13L(.5) & 12L(.4) & 12L(.3) & 11L(.2) & 15L(.1) & 4L(0) & 0 & 0 & 0 \\ 13L(.6) & 12L(.5) & 12L(.4) & 11L(.3) & 14L(.2) & 12L(.1) & 5L(0) & 0 & 0 \\ 13L(.7) & 12L(.6) & 12L(.5) & 11L(.4) & 14L(.3) & 11L(.2) & 13L(.1) & 5L(0) & 0 \\ 13L(.8) & 12L(.7) & 12L(.6) & 11L(.5) & 14L(.4) & 11L(.3) & 12L(.2) & 13L(.1) & 5L(0) \end{bmatrix} \begin{Bmatrix} Z_n(.1) \\ Z_n(.2) \\ Z_n(.3) \\ Z_n(.4) \\ Z_n(.5) \\ Z_n(.6) \\ Z_n(.7) \\ Z_n(.8) \\ Z_n(.9) \end{Bmatrix} +$$

$$\frac{i(M^2-2)}{2k\beta^3} \begin{Bmatrix} Z_n(.1) \\ Z_n(.2) \\ Z_n(.3) \\ Z_n(.4) \\ Z_n(.5) \\ Z_n(.6) \\ Z_n(.7) \\ Z_n(.8) \\ Z_n(.9) \end{Bmatrix} + \frac{1}{4k^2\beta} \begin{Bmatrix} Z_n'(.1) \\ Z_n'(.2) \\ Z_n'(.3) \\ Z_n'(.4) \\ Z_n'(.5) \\ Z_n'(.6) \\ Z_n'(.7) \\ Z_n'(.8) \\ Z_n'(.9) \end{Bmatrix} \tag{26}$$

$$\begin{Bmatrix} \bar{P}_n(.1) \\ \bar{P}_n(.2) \\ \bar{P}_n(.3) \\ \bar{P}_n(.4) \\ \bar{P}_n(.5) \\ \bar{P}_n(.6) \\ \bar{P}_n(.7) \\ \bar{P}_n(.8) \\ \bar{P}_n(.9) \end{Bmatrix} = \frac{\rho_0/\rho}{120} \begin{bmatrix} \bar{L}(0) & \bar{L}(.1) & \bar{L}(.2) & \bar{L}(.3) & \bar{L}(.4) & \bar{L}(.5) & \bar{L}(.6) & \bar{L}(.7) & \bar{L}(.8) \\ \bar{L}(.1) & \bar{L}(0) & \bar{L}(.1) & \bar{L}(.2) & \bar{L}(.3) & \bar{L}(.4) & \bar{L}(.5) & \bar{L}(.6) & \bar{L}(.7) \\ \bar{L}(.2) & \bar{L}(.1) & \bar{L}(0) & \bar{L}(.1) & \bar{L}(.2) & \bar{L}(.3) & \bar{L}(.4) & \bar{L}(.5) & \bar{L}(.6) \\ \bar{L}(.3) & \bar{L}(.2) & \bar{L}(.1) & \bar{L}(0) & \bar{L}(.1) & \bar{L}(.2) & \bar{L}(.3) & \bar{L}(.4) & \bar{L}(.5) \\ \bar{L}(.4) & \bar{L}(.3) & \bar{L}(.2) & \bar{L}(.1) & \bar{L}(0) & \bar{L}(.1) & \bar{L}(.2) & \bar{L}(.3) & \bar{L}(.4) \\ \bar{L}(.5) & \bar{L}(.4) & \bar{L}(.3) & \bar{L}(.2) & \bar{L}(.1) & \bar{L}(0) & \bar{L}(.1) & \bar{L}(.2) & \bar{L}(.3) \\ \bar{L}(.6) & \bar{L}(.5) & \bar{L}(.4) & \bar{L}(.3) & \bar{L}(.2) & \bar{L}(.1) & \bar{L}(0) & \bar{L}(.1) & \bar{L}(.2) \\ \bar{L}(.7) & \bar{L}(.6) & \bar{L}(.5) & \bar{L}(.4) & \bar{L}(.3) & \bar{L}(.2) & \bar{L}(.1) & \bar{L}(0) & \bar{L}(.1) \\ \bar{L}(.8) & \bar{L}(.7) & \bar{L}(.6) & \bar{L}(.5) & \bar{L}(.4) & \bar{L}(.3) & \bar{L}(.2) & \bar{L}(.1) & \bar{L}(0) \end{bmatrix} \begin{Bmatrix} 13Z_n(.1) \\ 12Z_n(.2) \\ 12Z_n(.3) \\ 11Z_n(.4) \\ 14Z_n(.5) \\ 11Z_n(.6) \\ 12Z_n(.7) \\ 12Z_n(.8) \\ 13Z_n(.9) \end{Bmatrix} \tag{27}$$

$$\begin{Bmatrix} \bar{\bar{P}}_n(.1) \\ \bar{\bar{P}}_n(.2) \\ \bar{\bar{P}}_n(.3) \\ \bar{\bar{P}}_n(.4) \\ \bar{\bar{P}}_n(.5) \\ \bar{\bar{P}}_n(.6) \\ \bar{\bar{P}}_n(.7) \\ \bar{\bar{P}}_n(.8) \\ \bar{\bar{P}}_n(.9) \end{Bmatrix} = \frac{\rho_0/\rho}{4} \begin{bmatrix} \bar{\bar{L}}_1(.1) & \bar{\bar{L}}_2(.1) & \bar{\bar{L}}_3(.1) & \bar{\bar{L}}_4(.1) & \bar{\bar{L}}_5(.1) & \bar{\bar{L}}_6(.1) & \bar{\bar{L}}_7(.1) & \bar{\bar{L}}_8(.1) & \bar{\bar{L}}_9(.1) & \bar{\bar{L}}_{10}(.1) \\ \bar{\bar{L}}_1(.2) & \bar{\bar{L}}_2(.2) & \bar{\bar{L}}_3(.2) & \bar{\bar{L}}_4(.2) & \bar{\bar{L}}_5(.2) & \bar{\bar{L}}_6(.2) & \bar{\bar{L}}_7(.2) & \bar{\bar{L}}_8(.2) & \bar{\bar{L}}_9(.2) & \bar{\bar{L}}_{10}(.2) \\ \bar{\bar{L}}_1(.3) & \bar{\bar{L}}_2(.3) & \bar{\bar{L}}_3(.3) & \bar{\bar{L}}_4(.3) & \bar{\bar{L}}_5(.3) & \bar{\bar{L}}_6(.3) & \bar{\bar{L}}_7(.3) & \bar{\bar{L}}_8(.3) & \bar{\bar{L}}_9(.3) & \bar{\bar{L}}_{10}(.3) \\ \bar{\bar{L}}_1(.4) & \bar{\bar{L}}_2(.4) & \bar{\bar{L}}_3(.4) & \bar{\bar{L}}_4(.4) & \bar{\bar{L}}_5(.4) & \bar{\bar{L}}_6(.4) & \bar{\bar{L}}_7(.4) & \bar{\bar{L}}_8(.4) & \bar{\bar{L}}_9(.4) & \bar{\bar{L}}_{10}(.4) \\ \bar{\bar{L}}_1(.5) & \bar{\bar{L}}_2(.5) & \bar{\bar{L}}_3(.5) & \bar{\bar{L}}_4(.5) & \bar{\bar{L}}_5(.5) & \bar{\bar{L}}_6(.5) & \bar{\bar{L}}_7(.5) & \bar{\bar{L}}_8(.5) & \bar{\bar{L}}_9(.5) & \bar{\bar{L}}_{10}(.5) \\ \bar{\bar{L}}_1(.6) & \bar{\bar{L}}_2(.6) & \bar{\bar{L}}_3(.6) & \bar{\bar{L}}_4(.6) & \bar{\bar{L}}_5(.6) & \bar{\bar{L}}_6(.6) & \bar{\bar{L}}_7(.6) & \bar{\bar{L}}_8(.6) & \bar{\bar{L}}_9(.6) & \bar{\bar{L}}_{10}(.6) \\ \bar{\bar{L}}_1(.7) & \bar{\bar{L}}_2(.7) & \bar{\bar{L}}_3(.7) & \bar{\bar{L}}_4(.7) & \bar{\bar{L}}_5(.7) & \bar{\bar{L}}_6(.7) & \bar{\bar{L}}_7(.7) & \bar{\bar{L}}_8(.7) & \bar{\bar{L}}_9(.7) & \bar{\bar{L}}_{10}(.7) \\ \bar{\bar{L}}_1(.8) & \bar{\bar{L}}_2(.8) & \bar{\bar{L}}_3(.8) & \bar{\bar{L}}_4(.8) & \bar{\bar{L}}_5(.8) & \bar{\bar{L}}_6(.8) & \bar{\bar{L}}_7(.8) & \bar{\bar{L}}_8(.8) & \bar{\bar{L}}_9(.8) & \bar{\bar{L}}_{10}(.8) \\ \bar{\bar{L}}_1(.9) & \bar{\bar{L}}_2(.9) & \bar{\bar{L}}_3(.9) & \bar{\bar{L}}_4(.9) & \bar{\bar{L}}_5(.9) & \bar{\bar{L}}_6(.9) & \bar{\bar{L}}_7(.9) & \bar{\bar{L}}_8(.9) & \bar{\bar{L}}_9(.9) & \bar{\bar{L}}_{10}(.9) \end{bmatrix} \begin{Bmatrix} s_1 \\ s_2 \\ s_3 \\ s_4 \\ s_5 \\ s_6 \\ s_7 \\ s_8 \\ s_9 \\ s_{10} \end{Bmatrix} \tag{28}$$

where $L(u)$ and $\bar{L}(u)$ are defined after equation (21) and $\bar{\bar{L}}_r(u)$ and $s_r$ are defined in appendix B (eqs. (B16) and (B15)).

The rows of the square matrix in equation (26), down to the row pertaining to $P_n(.5)$, were obtained by applying the integration rule given by equation (25a). In the remaining rows the contributions from the region $x>0.5$ were obtained by applying equation (25b). In equation (27) the integrating factors multiplying $Z_n$ in the column matrix were obtained by using equation (25a) between $x=0$ and $x=0.5$ and equation (25b) between $x=0.5$ and $x=1.0$. In appendix B the singular integral $\overline{\overline{P}}_n(x)$ presented after equation (22) is evaluated and the form of $\overline{\overline{P}}_n$ leading to equation (28) is derived.

Equations (26), (27), and (28) are summed in accordance with equation (22) to obtain the column matrix $\{p_n(x)\}$. By use of this column matrix and the integration rules of equation (25), the aerodynamic term $C_{mn}$ is obtained in the form

$$C_{mn}=\frac{1}{120}[13p_n(.1)Z_m(.1)+12p_n(.2)Z_m(.2)+12p_n(.3)Z_m(.3)+11p_n(.4)Z_m(.4)+14p_n(.5)Z_m(.5)+11p_n(.6)Z_m(.6)+12p_n(.7)Z_m(.7)+12p_n(.8)Z_m(.8)+13p_n(.9)Z_m(.9)] \quad (29)$$

where the integrating factors 13, 12, . . . 12, 13 were obtained in the same manner as those in equation (27). By means of equation (29), $C_{mn}$ can be evaluated for a given edge fixity and for particular values of $M$, $k$, and $\rho_0/\rho$.

### SOLUTION OF FLUTTER DETERMINANT

As previously stated, the conditions for flutter are determined from the nontrivial solutions of equation (14). Since equation (14) is complex, it may be solved directly for one complex unknown or two real unknowns. For a specific edge fixity the variables (see eq. (13)) in equation (14) are $1/\mu$ (the inverse of $\mu$ is preferred because $\mu$ becomes infinite for $\rho=0$), $\Omega$, $f$, $M$, $k$, and $\rho_0/\rho$. It is convenient to interpret the $\Omega$ of equation (13) as the complex quantity $(\omega_1/\omega)^2(1+ig)$ rather than $(\omega_1/\omega)^2$, where $g$ may be regarded as a structural damping coefficient. (For this use of $g$, see, for example, refs. 12 and 13.) Each of the various quantities on which equation (14) is dependent was varied to some extent, as will be discussed in the next section. A particular calculation was performed by setting values for $1/\mu$, $M$, $k$, $f$, and $\rho_0/\rho$ and solving for $\Omega$. Then, because it was one of the more easily varied parameters, $1/\mu$ was changed and again $\Omega$ was solved for. This procedure was continued until curves of $1/\mu$ and $(R.P.\Omega)^{1/2}$ plotted against $g$ passed through $g=0$. The value for $k$ was then changed and the procedure repeated. After sufficient variation of $1/\mu$ and $k$, curves could be established of $1/\mu$ against $2k_1=2k(R.P.\Omega)^{1/2}$ for particular values of the other parameters $M$, $g$, $f$, and $\rho_0/\rho$.

## RESULTS AND DISCUSSION

In the preceding sections a method of flutter analysis has been developed for a two-dimensional flat panel or plate held at its leading and trailing edges. The variables in the analysis are the number of modes or degrees of freedom the panel is assumed to have, Mach number (greater than 1.0), $1/\mu$, $2k_1=2k(R.P.\Omega)^{1/2}$, $g$, $f$, $\rho_0/\rho$, and edge fixity. The analysis conveniently yields stability boundaries in terms of $1/\mu$ and $2k_1$, which are used as the coordinates of most of the figures presented. These two parameters are given in terms of the properties of the panel and supersonic stream by

$$\left.\begin{aligned}\frac{1}{\mu}&=\frac{\rho}{\sigma}\frac{c}{\tau}\\ 2k_1&=\frac{\omega_1 c}{U}=\frac{K_1^2}{\sqrt{24(1-\nu^2)}}\frac{\tau}{c}\sqrt{\frac{\rho}{\sigma}\frac{E}{q}}\end{aligned}\right\} \quad (30)$$

where $\sigma$ is panel density, $q$ is dynamic pressure, and $K_1$ is the first-mode eigenvalue given in table I for clamped and pinned edges. Inasmuch as the various parameters in the analysis contain implicitly the panel properties ($E$, $\sigma$, $\nu$, and $\tau/c$), axial force $F$, air density, and speed of sound, the effects of varying these implicit properties can be obtained only by cross-plotting.

Some effects of the number of modes used in the analysis are studied by using two and then four modes of the clamped-edge panel with selected values of $M$, $g$, $f$, and $\rho_0/\rho$. In addition, $M$, $g$, $f$, and $\rho_0/\rho$ are varied in order to study their effects. To a lesser extent the pinned-edge panel is investigated for comparison with certain clamped-edge results.

The following table lists the conditions for which stability boundaries are given:

| Mach number, $M$ | Degrees of freedom | Structural damping coefficient, $g$ | Tension parameter, $f$ | Density ratio, $\rho_0/\rho$ |
|---|---|---|---|---|
| Clamped edge | | | | |
| 1.3 | 2 | 0 | 0 | 0 |
| | | | 0, 0.1, 0.5, 1.0 | 1.0 |
| | 4 | 0, 0.005, 0.025, 0.03, 0.05 | 0 | 0 |
| | | 0 | 0, 0.1, 0.5, 1.0 | 0 |
| $\sqrt{2}$ | 2 | 0, 0.002, 0.00375, 0.05 | 0 | 0 |
| 1.56 | 2 | 0 | 0 | 0 |
| | 4 | 0 | 0 | 0 |
| Pinned edge | | | | |
| $\sqrt{2}$ | 2 | 0, 0.003, 0.00475, 0.05 | 0 | 0 |

The results are first grouped according to Mach number and are later summarized and compared.

### RESULTS FOR MACH NUMBER OF 1.3

**Effects of two and four modes.**—Figure 2 gives the results for the clamped-edge panel for the simple case of two degrees of freedom (first and second modes) with $g=f=\rho_0/\rho=0$. The abscissa is the stiffness parameter $\omega_1 c/U=2k_1$ and the ordinate is the mass ratio $1/\mu$. An ordinate of zero represents the limiting case of $\rho=0$, or, in other words, the plate is vibrating in a vacuum. The two solid curves are the first- and second-mode stability boundaries as indicated. It was

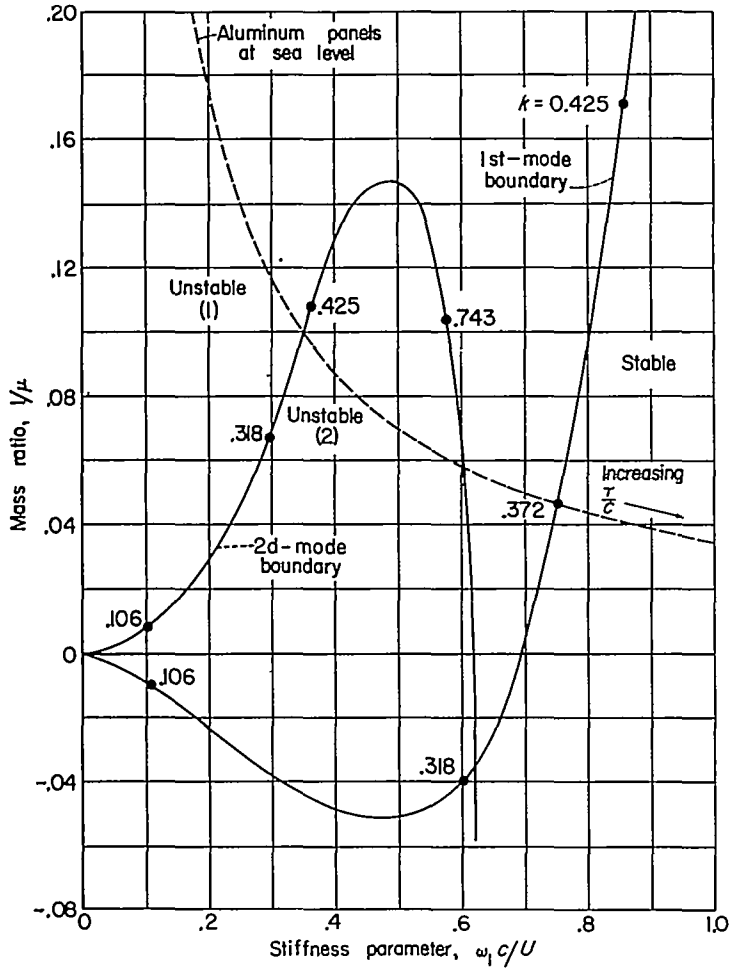


FIGURE 2.—Stability boundaries from a two-mode analysis for clamped-edge panels. $M=1.3$; $g=f=\frac{\rho_0}{\rho}=0$.

established by application of the Nyquist criterion (see, for example, ref. 14) as well as by interpretation of structural-damping results that the region to the right of the first mode boundary is stable, whereas the region to the left is unstable; furthermore, the region within the second-mode boundary is doubly unstable as indicated (unstable with regard to both boundaries). Values of the reduced frequency $k$ are indicated along both curves. The points at which the curves cross the abscissa correspond to vibration in a pure normal mode (flutter at the limiting condition of $\rho=0$).

It can be seen from equations (30), by taking the product of $1/\mu$ and $2k_1$, that a specified panel material, air density, and speed of sound are represented by a hyperbola such as the dashed curve of figure 2 with the panel thickness-chord ratio $\tau/c$ increasing to the right. The intersection of the hyperbola with the stability boundary fixes the value of $\tau/c$ for neutral stability. Thicker panels are stable and thinner panels are unstable. (The particular hyperbola shown is for aluminum panels in air with standard sea-level properties. For denser panels or less dense air, the hyperbola would be below the one shown.)

Some effects of the number of modes in the analysis were studied by including the first four normal modes, and the results are shown as the solid curves of figure 3. The dashed curves are the results for two modes from figure 2. With the addition of the third and fourth modes, the first-mode boundary is moved very slightly to the left (except where it crosses the abscissa) and is still the "critical" or decisive stability boundary separating the stable from the unstable region. The second-mode boundary is also only moderately affected. Within the already unstable region there now exist third-mode and fourth-mode boundaries which are closely analogous in appearance and character to the first- and second-mode boundaries, respectively. The unstable region is divided by three of the boundaries, into regions of different degrees of instability as indicated by the numbers in parentheses ranging from (1) to (4). (The points at which the

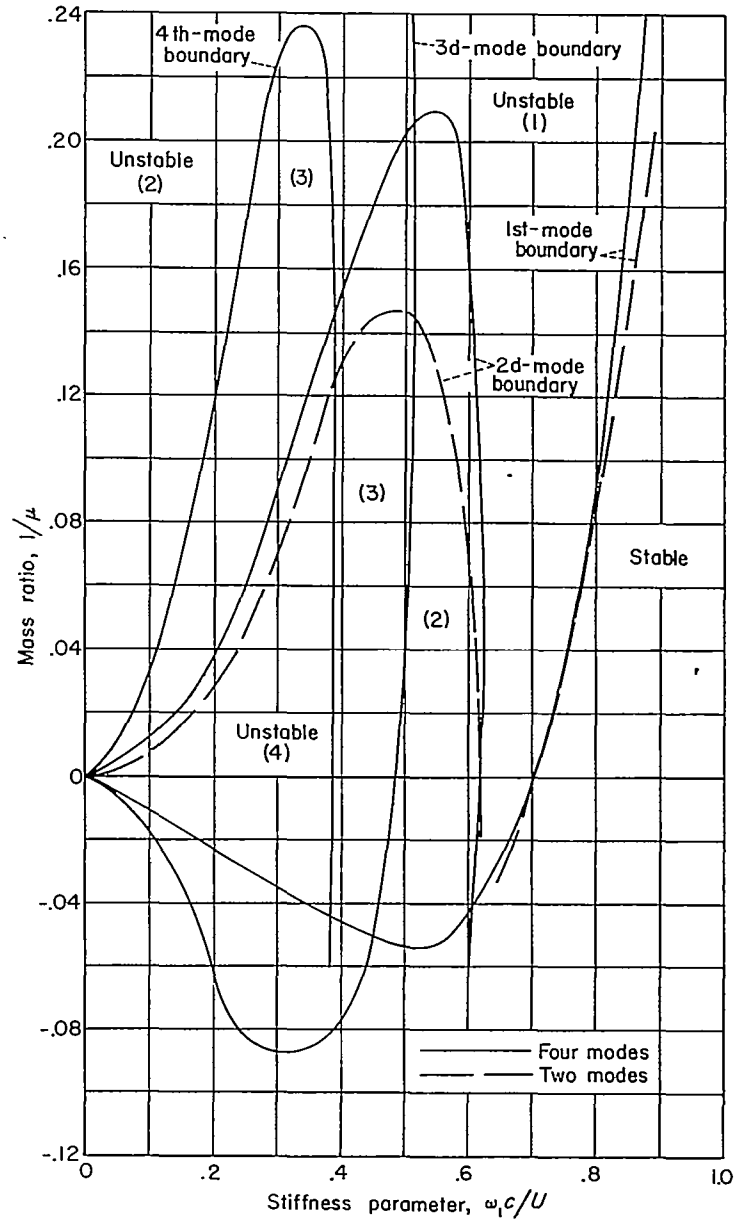


FIGURE 3.—Stability boundaries from two-mode and four-mode analyses for clamped-edge panels. $M=1.3$; $g=f=\frac{\rho_0}{\rho}=0$.

various boundaries cross the abscissa have the same significance as before.) These results indicate that two modes give a decisive stability boundary which is a close approximation to that for a large number of modes, at least for the conditions $g=f=\rho_0/\rho=0$ and $M=1.3$.

**Effects of structural damping coefficient $g$.**—Figures 4 (a) and 4 (b) show the first-mode and second-mode boundaries (from a four-mode analysis) for various values of $g$ (taken to be the same for all modes). Third- and fourth-mode boundaries are affected by $g$ in a manner similar to that of the first and second modes, respectively, and are not shown. The second-mode boundary of figure 4 (b) vanishes completely when $g$ becomes slightly greater than 0.025, and for all positive values of $g$ it remains in the unstable region to the left of the first-mode boundary. Included in figure 4 is the dashed hyperbola from figure 2. Since the thickness-chord ratio $\tau/c$ decreases to the left in the figure, the abscissas of the intersections of the hyperbola with the stability boundaries in figure 4 (a) show the proportional reduction in thickness required to prevent flutter as $g$ increases.

**Effects of tension.**—Tension has a marked effect on the stability boundaries, as shown in figures 5 (a) and 5 (b). Figure 5 (a) shows the pertinent segments of the first-, second-, third-, and fourth-mode stability boundaries for $g=0$ and for the three values 0.1, 0.5, and 1.0 of the tension parameter $f$. As $f$ increases, all the boundaries move to the left, and the thickness required to prevent flutter is decreased. Furthermore, as $f$ increases, the first-mode boundary moves to the left more rapidly than the higher mode boundaries so that the rightmost boundary, separating stable from unstable regions, is one of the higher mode boundaries. For example, for $f=1.0$ in figure 5 (a), the third-mode boundary is farthest to the right. This trend is not surprising since application of tension to the clamped-edge plate causes the largest percentage increase in the first natural frequency, the next largest in the second natural frequency, and so on. Thus, it appears that the inclusion of only two modes in a flutter analysis may not be sufficient when the plate is subjected to tension. Inasmuch as the stiffness parameter $2k_1$ and the tension parameter $f$ are both

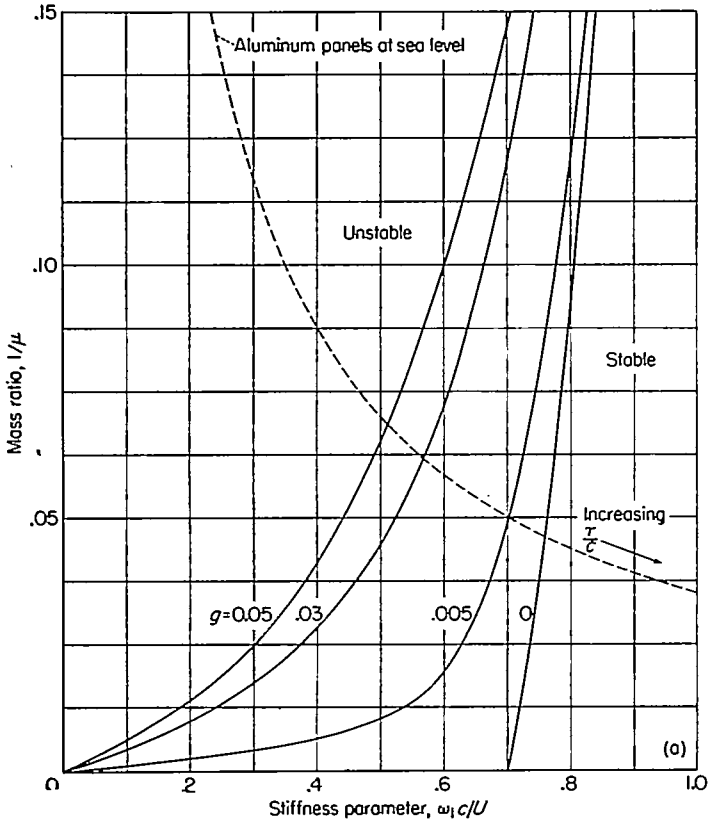


(a) First-mode boundary.

FIGURE 4.—First-mode and second-mode stability boundaries from a four-mode analysis for clamped-edge panels for various values of structural damping coefficient $g$. $M=1.3$; $f=\frac{\rho_0}{\rho}=0$.

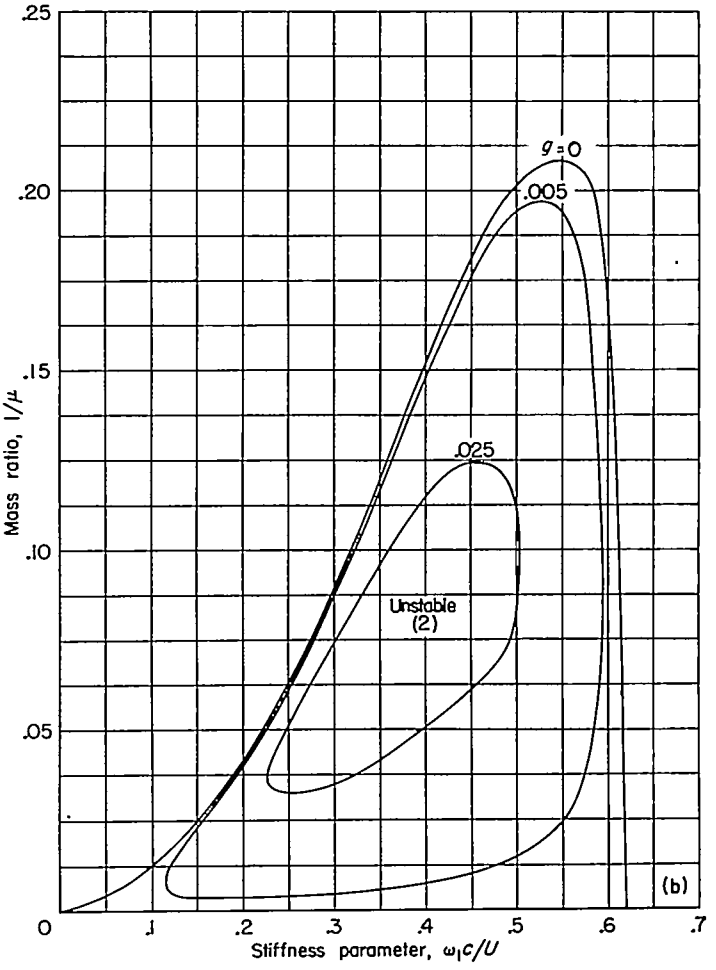


(b) Second-mode boundary.

FIGURE 4.—Concluded.

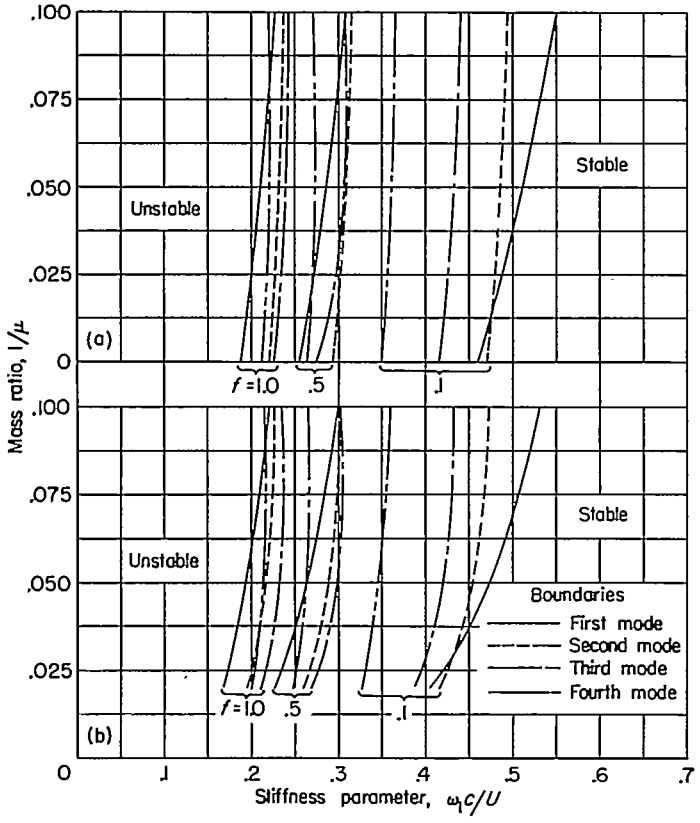


(a) $g=0$.
(b) $g=0.005$.

FIGURE 5.—Stability boundaries from a four-mode analysis for clamped-edge panels for three values of the tension parameter $f$. $M=1.3$; $\frac{\rho_0}{\rho}=0$.

based on the first natural frequency of the panel without tension, the shift of the boundaries is due solely to the tensile force $F$.

Figure 5 (b) shows segments of the first-, second-, third-, and fourth-mode boundaries with $f=0.1$, 0.5, and 1.0 for $g=0.005$. By comparing figures 5 (b) and 5 (a) it can be seen that $g$ has a marked effect for the smaller values of $f$ but its effect diminishes as $f$ increases.

**Effects of still air below panel.**—The one remaining parameter to be considered at $M=1.3$ is $\rho_0/\rho$, the ratio of the density of the still air below the panel to the density of the supersonic stream above. In the preceding results this ratio was zero. The effect of increasing $\rho_0/\rho$ to 1.0 will now be examined. For the sake of simplicity and convenience, only a two-mode analysis is made. Effects of structural damping and tension are also included.

Figure 6 (a) shows first- and second-mode boundaries for $\rho_0/\rho=1$ as solid curves and, for comparison, the dashed boundaries for $\rho_0/\rho=0$ from figure 2. Just as with the other results, the points where the boundaries cross the abscissa correspond to pure-mode resonance in a vacuum. At these crossings the imaginary part of $C_{nn}$ passes through zero. This imaginary part is a measure of aerodynamic damping. In the previous calculations $C_{nn}$ consisted only of $I_{nn}$, whereas, for $\rho_0/\rho=1.0$, $C_{nn}$ also contains $\bar{I}_{nn}+\bar{\bar{I}}_{nn}$ (see eq. (23)). By comparison of the solid and dashed curves on figure 6 (a) it can be seen that, as a consequence, the first-mode boundary has moved to the left by about 20 percent but the second-mode boundary has changed relatively little.

Such an effect of still air might be expected since, for the same maximum panel amplitude, a first-mode vibration radiates into the still-air region a greater amount of energy per cycle than does a second-mode vibration. (With regard to the radiation of sound from a piston in a plane wall, specifically for the case of a piston with nonrigid face, p. 336 of ref. 15 gives the result that, at frequencies which are small compared with the ratio of the speed of sound to $2\pi$ times the piston radius, the pressure on the piston is approximately uniform and nearly proportional to the average velocity of the piston. Since the average velocity of the second mode and all other antisymmetric modes is zero, the pressure due to these modes is nearly zero and, accordingly, almost no work is being done on the still air.) From the fact that net energy can never pass from the still air into the panel, it does not follow, however, that the still air necessarily has a stabilizing effect in all cases. Conceivably, the still air could act to modify the flutter mode so that more energy would be extracted from the supersonic stream, and thus contribute toward an instability. Apparently such is the case in figure 6 (a), where the solid second-mode curve is above the dashed second-mode curve. The fact that dissipation of energy into the still air is not necessarily stabilizing should not be surprising, inasmuch as another means of energy dissipation, structural damping, is usually stabilizing but sometimes destabilizing.

As can be observed in figure 6 (a), the first-mode boundary has moved to the left of the second-mode boundary in the region of small mass ratio; in this region the second-mode boundary becomes critical.

Figure 6 (b) shows the effects of structural damping on the first-mode boundary, which for $g=0$ is shown more completely in figure 6 (a). Curves are included for $g=0$, 0.005, 0.03, and 0.05. For values of $g$ larger than about 0.025 the second-mode boundary vanishes as it did previously with $\rho_0/\rho=0$ in figure 4 (b), and only the first-mode boundary remains. The dashed hyperbola for aluminum at sea level is included in figure 6 (b), and it can be seen that a plate with zero structural damping would have to be about 30 percent thicker than one with $g=0.05$ in order to prevent flutter.

Figure 7 shows the effects of the tension parameter $f$ for $\rho_0/\rho=1$ and $g=0$. Both first- and second-mode boundaries are shown for $f=0$, 0.1, 0.5, and 1.0. In this case, just as

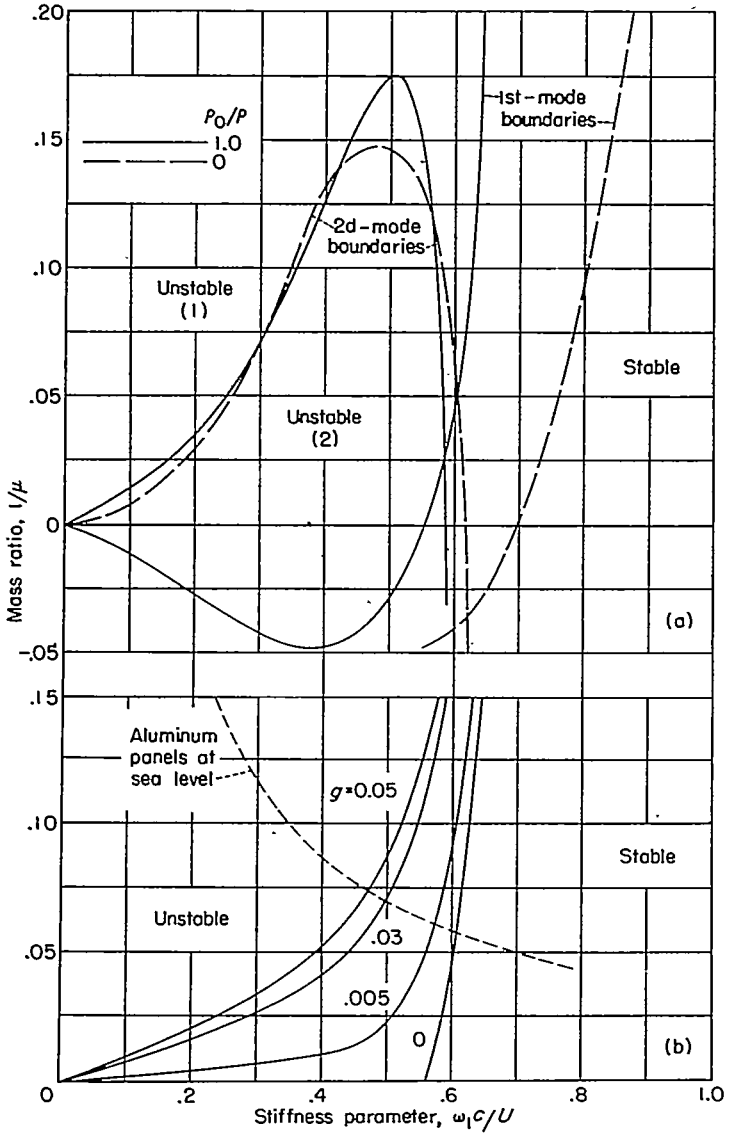


(a) First-mode and second-mode boundaries for $g=0$.

(b) First-mode boundary for various values of $g$.

FIGURE 6.—Stability boundaries from a two-mode analysis for clamped-edge panels for various values of $g$. $M=1.3$; $f=0$; $\frac{\rho_0}{\rho}=0$ and 1.0.

with $\rho_0/\rho=0$, tension causes a marked reduction in the thickness required to prevent flutter. Furthermore, if more than two modes had been included, tension would have resulted in a higher mode boundary farther to the right than the curves shown for the higher values of $f$.

### RESULTS FOR MACH NUMBER OF $\sqrt{2}$

**Clamped-edge panels.**—Figure 8 (a) shows the stability boundaries obtained from a two-mode analysis for clamped-edge panels at $M=\sqrt{2}$ with $f=\rho_0/\rho=0$ for various values of $g$. Included in the figure is the dashed hyperbola appropriate to this Mach number for aluminum panels in sea-level air. From a comparison of figure 2 and the curves of figure 8 (a)

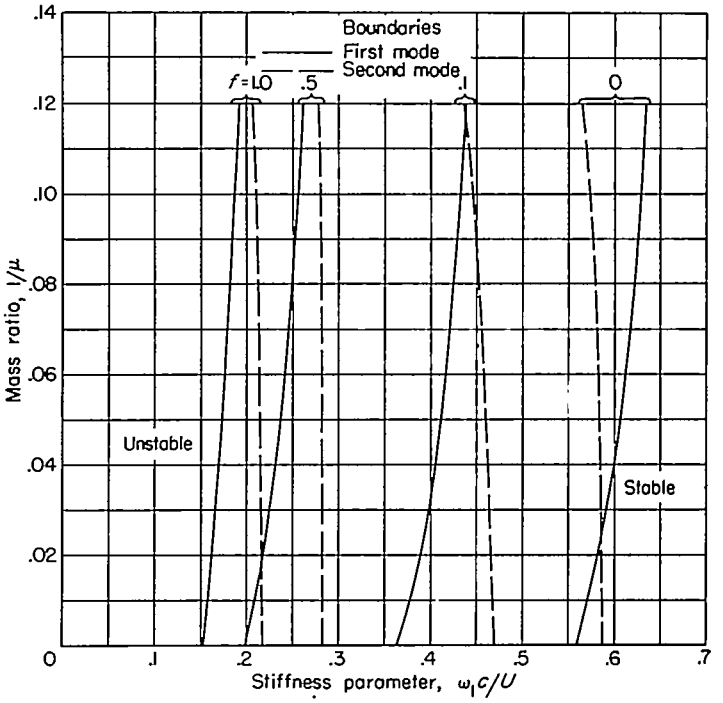


FIGURE 7.—Stability boundaries from a two-mode analysis for clamped-edge panels for various values of $f$. $M=1.3$; $g=0$; $\frac{\rho_0}{\rho}=1.0$.

for $g=0$, the first-mode boundary of figure 2 appears to have moved into the positive mass-ratio region and the second-mode boundary appears to be moving toward the negative mass-ratio region. Such is the case, but, inasmuch as the flutter frequencies on the upper boundary of figure 8 (a) are about midway between the first and second natural frequencies, this boundary can now be referred to only loosely as a "first-mode" boundary. The lower boundary is still readily identified as a second-mode boundary and the intersection with the abscissa corresponds to vibration in a pure second mode.

In contrast to the situation at $M=1.3$, the second-mode boundary for $g=0$ is now decisive for panels represented by the dashed hyperbola. Values of thickness to the right of the second-mode boundary are stable and, in addition, a small range of thickness values is stable between he upper and second-mode boundaries.

The curves in figure 8 (a) for positive values of $g$ show that the region of instability within the second-mode boundary is reduced for small values of $g$ (as for $M=1.3$) and vanishes when $g$ is slightly greater than 0.00375, but that small values of $g$ increase the region of instability associated with the upper boundary. This effect of $g$ on the upper boundary is in marked contrast to its effect on the first-mode boundary at $M=1.3$. (See fig. 4 (a).) The differing effects of structural damping at $M=1.3$, $M=\sqrt{2}$, and $M=1.56$ are considered further in the section on "Variations With Mach Number."

**Pinned-edge panels.**—In order to indicate effects of edge

fixity, boundaries are shown in figure 8 (b) for conditions identical to those of figure 8 (a) except that the edges are pinned rather than clamped. The boundaries for $g=0$, which are given incompletely in reference 5 and thereby lead to the conclusion that only a small range of panel thickness is stable at $M=\sqrt{2}$, have been extended to higher frequencies with the result that sufficiently thick panels are also found to be stable. The effect of structural damping on both boundaries in figure 8 (b) is very similar to that in figure 8 (a). The dashed hyperbola appropriate to pinned-edge aluminum panels in sea-level air is included in the figure. The hyperbolas of figures 8 (a) and 8 (b) are located differently because of the different values for the first-mode eigenvalue $K_1$ of equation (30) for pinned and clamped edges. (See table I.) From the intersection of the dashed hyperbolas with the stability boundaries in the two figures, it can be determined that a pinned-edge panel must be somewhat thicker than a clamped-edge panel in order to be flutter free but not nearly as thick as might be expected from a simple comparison of the first natural frequencies. Values of the reduced frequency $k$ are indicated along each of the boundaries of figure 8.

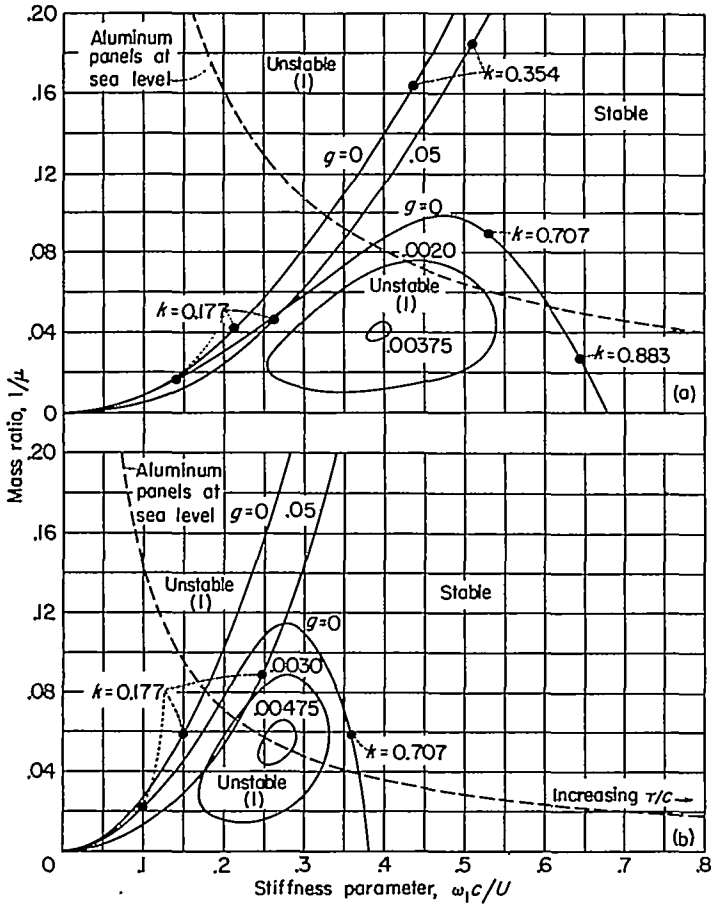


(a) Clamped-edge panel.
(b) Pinned-edge panel.

FIGURE 8.—Stability boundaries from a two-mode analysis for clamped-edge and pinned-edge panels for various values of $g$. $M=\sqrt{2}$; $f=\frac{\rho_0}{\rho}=0$.

Based on what occurred at $M=1.3$ (see fig. 3), there is the possibility that for $g=0$ the fourth-mode boundary from a four-mode analysis would alter the stability picture in both figures 8 (a) and 8 (b) in the relatively unimportant narrow range of stability between the boundaries shown for $g=0$. This minor effect of the fourth-mode boundary is expected to disappear for values of $g$ greater than about 0.005 and, therefore, a four-mode analysis was not made for this Mach number.

### RESULTS FOR MACH NUMBER OF 1.56

**Effects of two and four modes.**—As in the case of $M=1.3$, stability boundaries were obtained first for two and then for four degrees of freedom with $g=f=\rho_0/\rho=0$. These boundaries appear in figure 9 as dashed curves for two modes and solid curves for four modes. Values of the reduced frequency $k$ are indicated along the boundaries. The stable region is again to the right, and on the left the degree of instability is indicated in parentheses for the four-mode analysis.

The two-mode results in figure 9 continue the trend noted in the preceding section from comparison of the curves of figure 2 and those of figure 8 (a) for $g=0$. The second-mode

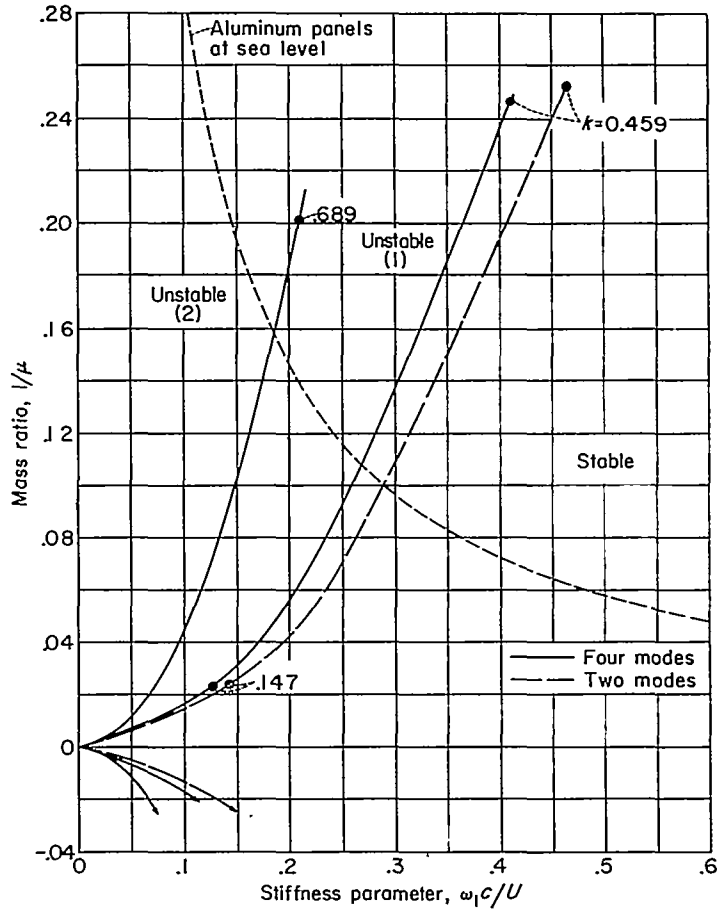


FIGURE 9.—Stability boundaries from two-mode and four-mode analyses for clamped-edge panels. $M=1.56$; $g=f=\frac{\rho_0}{\rho}=0$.

boundary has moved entirely into the negative mass-ratio region. The upper boundary has moved higher in the positive mass-ratio region, and the flutter frequencies along it, which in figure 8 (a) were midway between the first and second natural frequencies, are now closer to the second. For this reason the upper boundary, which was loosely identified as a "first-mode" boundary in the discussion of figure 8 (a), will now be referred to as a "second-mode" boundary.

A further point of difference between the results at $M=1.3$ and $M=1.56$ is that the addition of the third and fourth modes at $M=1.56$ shifts the decisive stability boundary to the left by about 10 percent, whereas at $M=1.3$ the shift is insignificant. (Compare figs. 3 and 9.) Although this shift indicates that the two-mode result is not well converged, the two-mode boundary is conservative; that is, it requires a greater thickness to prevent flutter. (As with two modes, when four modes are used, half of the stability boundaries fall in the negative mass-ratio region.)

**Effects of structural damping coefficient $g$.**—No curves are shown to indicate effects of structural damping at a Mach number of 1.56, the reason being that, for moderate values of the coefficient $g$, ranging at least up to 0.05, the stability boundaries fall virtually on top of those for $g=0$. The major effect of structural damping is a moderate change in flutter frequency.

**Effects of tension and of still air below panel.**—Effects of tension have not been determined, but tension is expected to have essentially the same favorable stiffening effect at all Mach numbers as at $M=1.3$. The effect of still air behind the panel has also not been determined, but this effect is expected to be less than at $M=1.3$ for two reasons: First, the air beneath the panel acts primarily as an energy absorber and one means of energy absorption, structural damping, has been found ineffective in shifting the stability boundaries. Second, on the decisive boundary the flutter mode appears to be predominantly the second natural panel mode, and it was found that at $M=1.3$ the second-mode boundary is changed only slightly by increasing $\rho_0/\rho$ from 0 to 1.

### VARIATIONS WITH MACH NUMBER

The foregoing results have been presented for particular Mach numbers. In an effort to clarify some of the anomalies that have been noted in these results, figures 10 to 12 are presented. Figure 10 shows the panel thickness-chord ratio required to prevent flutter as a function of $M$ for clamped-edge panels with $g=f=\rho_0/\rho=0$. The curves apply to aluminum panels in standard sea-level air. The values at $M=1.3$, $\sqrt{2}$, and 1.56 were obtained from figures 2 and 8 (a) and the two-mode results of figure 9. The shape of the curves between these known points is estimated. The stable region is above or to the right of the shaded boundaries.

The boundary which is labeled "first-mode" on one end and "second-mode" on the other has flutter frequencies which progress from slightly above the first natural frequency to somewhat below the second natural frequency as the Mach number is increased. (See previous discussions concerning figs. 2, 8 (a), and 9.) The boundary labeled "second-mode" has flutter frequencies slightly below the second natural frequency throughout.

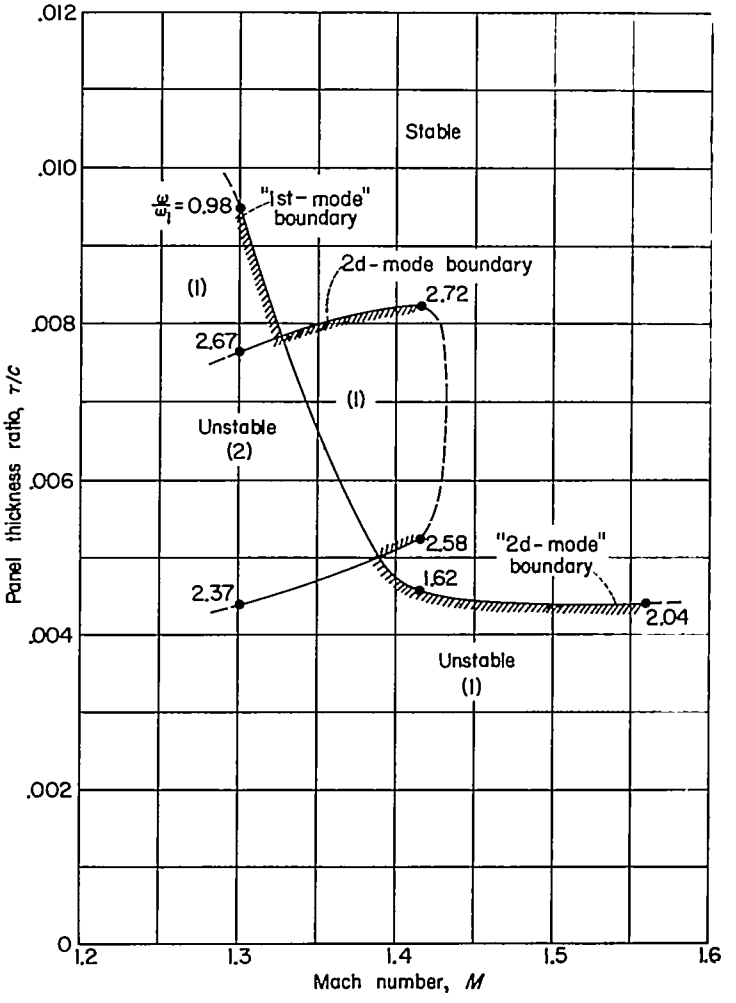


FIGURE 10.—Minimum panel thickness ratio $\tau/c$ required to prevent flutter as a function of Mach number for clamped-edge aluminum panels in sea-level air. $g=f=\frac{\rho_0}{\rho}=0$.

Figure 10 shows the second-mode stability boundary to be decisive in the Mach number range from slightly above 1.30 to slightly above $\sqrt{2}$. As the structural damping $g$ is increased from zero, the second-mode boundary shrinks to the left leaving the "first-mode"—"second-mode" boundary decisive throughout the range of $M$ shown. For example, for a value of $g$ slightly greater than 0.0038 the second-mode boundary does not exist at $M=\sqrt{2}$ (see fig. 8 (a)), and for a value of $g$ slightly greater than 0.025 it does not exist at $M=1.3$ (see fig. 4 (b)).

These effects of $g$ on the second-mode boundary are illustrated in figure 11, which contains cross plots of $g$ against $\tau/c$ obtained from the intersections of the dashed hyperbolas (for aluminum panels in sea-level air) with the boundaries for constant $g$ such as shown in figures 4, 8 (a), and 9. Figure 11 also shows that an increase in $g$ from

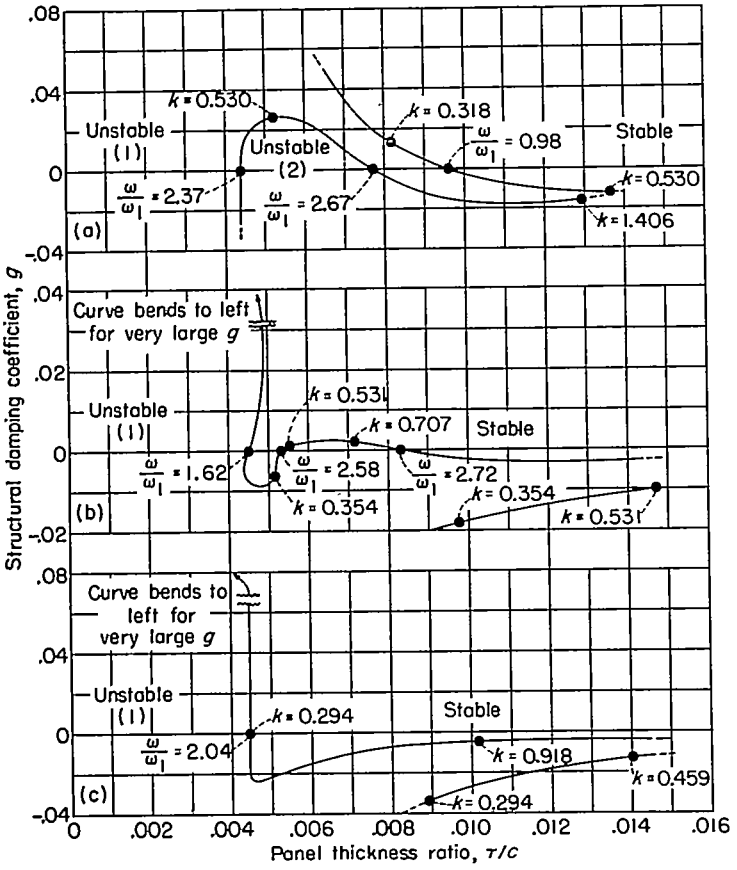


(a) $M=1.30$.
(b) $M=\sqrt{2}$.
(c) $M=1.56$.

FIGURE 11.—Structural damping coefficient $g$ as a function of panel thickness ratio $\tau/c$ from a two-mode analysis for clamped-edge aluminum panels in sea-level air. $f=\frac{\rho_0}{\rho}=0$. (Refer to dashed hyperbolas in figs. 2, 8 (a), and 9.)

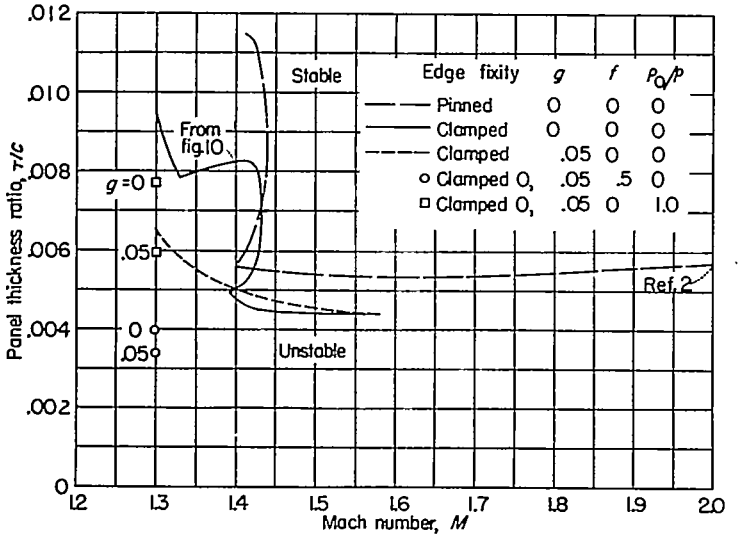


FIGURE 12.—Minimum panel thickness ratio $\tau/c$ required to prevent flutter as a function of Mach number for aluminum panels in sea-level air.

zero would cause the "first-mode"—"second-mode" boundary of figure 10 to drop markedly at $M=1.3$, rise slightly at $M=\sqrt{2}$, and remain essentially unchanged at $M=1.56$. The ratios of flutter frequency to the first natural frequency $\omega/\omega_1$ are indicated for each of the crossings and tend to show more clearly the connection between figures 10 and 11. (Values of $\omega/\omega_1$ near $\omega_2/\omega_1$, which is approximately 2.76, are associated with the second-mode boundary and values between 1.0 and 2.05 are associated with the "first-mode"—"second-mode" boundary.) A complete understanding of the manner in which the curves change character and position with Mach number, particularly between $M=1.3$ and $M=\sqrt{2}$, requires more calculation than presented herein.

Figure 12, which has the same ordinates as figure 10, is presented for the purpose of summarizing some effects of all the parameters investigated. The results shown are based on two modes, except in the case of tension where only four-mode results are known. The results again apply to aluminum panels in sea-level air. The figure shows as a solid curve the shaded boundary from figure 10 for clamped-edge panels and as a short-dash curve the effect on this boundary of increasing $g$ from 0 to 0.05. The third (long-dash) curve is for pinned-edge panels with $g=0$, the value at $M=2$ having been obtained from reference 2. The points at $M=\sqrt{2}$ were obtained from figure 8 (b) and the upper (second-mode) curve was patterned after that for clamped-edge panels. As a matter of interest, points are included in figure 12 at $M=1.3$ for clamped-edge panels and indicate the effects of tension ($f=0.5$) and of still air below the panel ($\rho_0/\rho=1.0$) for $g=0$ and $g=0.05$.

Some effects of the various parameters can be assessed from figure 12. The overall result is that $\tau/c$ is highest in the low supersonic Mach number range and suggests that this range is the more critical from a design standpoint. Structural damping is seen to have a large favorable effect near and below $M=\sqrt{2}$. Although rather influential at $M=1.3$, the still air below the panel is expected to have less effect at $M=\sqrt{2}$ and 1.56. Tension, which is seen to have a large favorable effect at $M=1.3$, is expected to be similarly effective for all Mach numbers. In this connection, it might be mentioned that one means of producing tension is by a static-pressure difference between the upper and lower panel surfaces, particularly for the case where the panel leading and trailing edges are prevented from moving toward each other. A comparison of the results for the edge fixities, pinned and clamped, is of interest because the edge fixity of actual panels falls somewhere between.

### COMPARISON WITH OTHER THEORETICAL WORK

In reference 2 the conclusion is reached that all panels, regardless of thickness, are unstable for supersonic Mach numbers less than $\sqrt{2}$. This result and the more plausible results of reference 2 for $M>\sqrt{2}$ are based on air forces expanded to the first power of the frequency of oscillation. In reference 5 the necessity of including higher order frequency terms for Mach numbers near $\sqrt{2}$ is pointed out, and

stability boundaries, based on exact linearized unsteady air forces, are presented for $M=\sqrt{2}$ and $M=2$. One boundary is obtained at $M=2$ which agrees well with the comparable result from reference 2, whereas two boundaries are obtained at $M=\sqrt{2}$. The boundaries at $M=\sqrt{2}$, because they are not carried high enough in frequency, are interpreted in reference 5 as showing that stability is possible only for a small range of panel thickness at this Mach number. The results of reference 2 for $M<\sqrt{2}$ are not questioned in reference 5.

In the present report, stability boundaries are computed for $M=\sqrt{2}$ and for Mach numbers above and below this value (namely, $M=1.3$ and $M=1.56$). In view of the findings of references 2 and 5, perhaps the most noteworthy result of the present investigation is that, for the Mach numbers treated and probably throughout the supersonic range, sufficiently thick panels are stable.

In references 2 and 5 and the present report, $M=\sqrt{2}$ appears as a transitional value. The transition is evidenced herein by the contrasting behavior of the stability boundaries at $M=1.3$ and $M=1.56$. Some understanding of why a Mach number of $\sqrt{2}$ is transitional can be had by examining matrix equation (26). The term $\frac{i(M^2-2)}{2k\beta^3}\{Z_n\}$ of equation (26), being the entire first-order frequency contribution to the damping, is dominant at low frequencies. This term appears to control the slope, at low frequencies, of the eventually decisive stability boundary and changes sign as $M$ passes through $\sqrt{2}$. When $M<\sqrt{2}$, the slope is negative for low frequencies, but as the frequency increases the slope eventually becomes positive because of the higher order frequency effects (for example, in fig. 2). Because only first-order frequency effects are included, in essence only the beginning portions of the stability boundaries for $M<\sqrt{2}$ are obtained in reference 2, and, as a consequence, the conclusion is reached that all panels are unstable below this Mach number. For $M>\sqrt{2}$ the slope of the decisive stability boundary starts out positive and becomes more so as the frequency increases. (See fig. 9.) If aspect ratio were included in the present treatment (by considering three-dimensional rather than two-dimensional panels), a reduction in aspect ratio would probably tend to eliminate the initial negative slope of the eventually decisive stability boundary for $M<\sqrt{2}$ and increase the initial positive slope for $M>\sqrt{2}$. This effect of aspect ratio is expected because, in general, a reduction in aspect ratio results in an increase in aerodynamic damping with a consequent enlargement of regions of stability.

In reference 7, which treats a different problem (namely, an infinite two-dimensional panel on equally spaced supports), the result was also obtained that somewhere in the supersonic Mach number range a panel will flutter regardless of its thickness. The conclusion was reached that stability is not possible at supersonic Mach numbers less than about 1.25 and that at higher Mach numbers a sufficient increase in thickness will always render a stable panel unstable. However, it was observed that over a large portion of the predicted region of instability the flutter was of an extremely mild character, since a large number of oscillations were required to double the amplitude. With the hope of eliminating the large region of mild instability, small amounts of viscous damping were included. Contrary to expectations, thick panels remained unstable for the example given at $M=1.8$.

As part of the viscous-damping investigation, the results were interpreted so as to determine regions of stability and instability. As shown in figure 10 of reference 7, an apparent conflict with the results of Nyquist diagrams was found. (The Nyquist diagram concept is used in general in reference 7 for determining stability.) This conflict is based on the assumption that most investigators interpret structural-damping results according to the concept that removal of damping tends to destabilize. This assumption is incorrect, however, and no such simple criterion holds true for interpreting structural-damping results. A feature to be noted in the example chosen in reference 7 to illustrate the apparent conflict is the existence of infinite singularities in the air forces at the end points of the boundaries ($g=0$, 0.01, and 0.03) on the right in figure 9 of the reference (designated type B loci therein). By way of explanation, such singularities occur in the linearized-flow treatment because a traveling wave of panel deflection is moving at a speed corresponding to $M=1$ relative to the air above or below the panel.

In this analysis the question of stability was investigated by means of both the structural-damping concept and the Nyquist diagram concept. The structural-damping results in every case agreed with the Nyquist diagram results. Incidentally, in using the Nyquist concept, knowledge of the aerodynamic forces for all frequencies from minus infinity to plus infinity is required. Thus, the concept is not applicable, in general, when the air forces are approximated by a few terms of a power-series expansion in the frequency of oscillation.

## COMPARISON WITH EXPERIMENT

A few experimental results on the flutter of flat and buckled panels are available for comparison with the theory of the present report for flat panels and that of reference 3 for buckled panels. Reference 16 gives experimental results at $M=1.3$ for panels 11.62 inches long in the stream direction and 8 inches wide that were held by clamping the leading and trailing edges. In figure 13, the results of reference 16 at $M=1.3$, together with data more recently obtained in the Langley supersonic flutter apparatus on both flat and buckled panels at other Mach numbers, are compared with theory. The results are presented in terms of the thickness-chord ratio $\tau/c$ needed to prevent flutter of aluminum-alloy panels at an altitude of 25,000 feet as a function of Mach number. These points were obtained from tests of panels of different thicknesses (see, for example, ref. 16) and represent the thinnest panels which did not flutter. (Where necessary, experimental data were adjusted to a pressure altitude of 25,000 feet with the relation $\tau/c=(\tau/c)_r(q/q_r)^{1/3}$. The subscript $r$ refers to the experimental conditions.)

In figure 13, the solid curve is the flutter boundary for flat panels obtained from the present theory and the square symbols are the corresponding experimental results. The

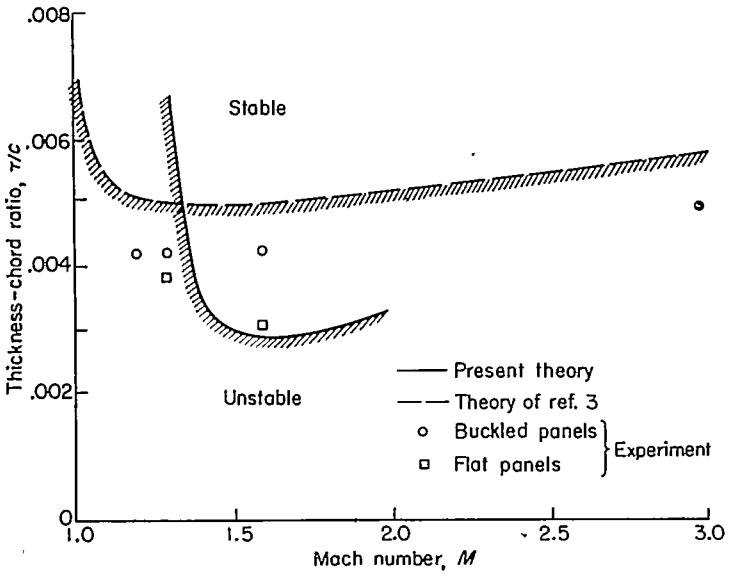


FIGURE 13.—Minimum panel thickness ratio $\tau/c$ required to prevent flutter of aluminum-alloy panels at 25,000-ft altitude.

dashed curve is the static-stability boundary for buckled panels, proposed as a flutter boundary in reference 3, and the circles are the associated experimental results. The theoretical curves are seen to increase rather sharply near Mach number 1.0. For buckled panels the increase is due to the use of steady-state linearized air forces which become infinite at $M=1$. For flat panels the increase is thought to be associated with a change in flutter mode and decreased aerodynamic damping. The curve for flat panels would have a finite ordinate at $M=1.0$.

As can be seen from figure 13, buckled panels have been fluttered up to a Mach number of 3. Flat panels were not fluttered over the same range because buckled panels appeared to be more susceptible to flutter, in general, and during a test it was difficult to prevent the thin, flat panels from buckling due to heating. (A temperature rise of 5° to 10° F was sufficient to induce buckling in many panels.)

The agreement between theory and experiment for both flat and buckled panels is surprisingly good, inasmuch as the experiments were made on panels with a width-length ratio of 0.69, whereas the theories are for two-dimensional panels.

## CONCLUDING REMARKS

A Rayleigh type analysis involving chosen modes of the panel as degrees of freedom has been used to treat the flutter of a two-dimensional flat panel supported at its leading and trailing edges and subjected to a middle-plane tensile force. The panel had a supersonic stream passing over its upper surface and still air below. The aerodynamic forces due to the supersonic stream were obtained from the theory for linearized two-dimensional unsteady flow and the forces due to the still air were obtained from acoustical theory. The still air beneath the panel was treated on the assumption that the still-air reservoir extended to infinity. Accordingly, once acoustic energy was radiated into this region, none of it was ever reflected. Such a situation is, of course, not the same as for a panel on a closed body but represents a first approximation for many practical cases.

In order to study the effect of increasing the number of modes in the analysis, two and then four modes were employed. The modes used were the first four natural modes of the panel in a vacuum with no tensile force acting. The analysis included the variables: Mach number $M$, structural damping, tensile force, density of the still air, and edge fixity (clamped and pinned). For certain combinations of these variables, stability boundaries were obtained which can be used to determine the panel thickness required to prevent flutter for any panel material and altitude.

In contrast to some previous panel flutter investigations, the present results show that sufficiently thick panels are flutter free for the Mach numbers treated and suggest that this is true throughout the supersonic speed range. The low supersonic Mach numbers were found to be most critical from a design standpoint in the range examined (from $M=1.3$ to $M=2.0$). Tension was shown at $M=1.3$ to have a marked favorable effect (also expected at all Mach numbers) in reducing the thickness required to prevent flutter, and it was pointed out that one means of producing tension is by a static pressure difference between the upper and lower surfaces of the panel. Small amounts of structural damping were found to have a pronounced beneficial effect near and below $M=\sqrt{2}$ and essentially no effect at $M=1.56$. In the neighborhood of $M=\sqrt{2}$ a small change in either Mach number or structural damping was found to cause an abrupt change in the thickness required to prevent flutter. At $M=\sqrt{2}$ a pinned-edge panel must be somewhat thicker than a clamped-edge panel in order to be flutter free: Still air below the panel was taken into account only at $M=1.3$ and was shown to have a moderate beneficial effect. For $M>\sqrt{2}$ the still air is expected to have little effect because for this Mach number range the flutter mode is predominantly the second natural mode, which radiates very little energy into the still air.

The theories of the present report for flat panels and of Isaacs for buckled panels were compared with a few experimental results on panels clamped at leading and trailing edges over the Mach number range 1.2 to 3.0. The agreement was surprisingly good inasmuch as the experiments were made on panels with a width-length ratio of 0.69, while the theories are for two-dimensional panels. Over the Mach number range of the experiments it was found that buckled panels had to be thicker than flat panels in order not to flutter. The effect of restraining flat or buckled panels on all four edges has not been investigated. Such restraint together with variation of width-length ratio will probably have a significant effect on the thickness required to prevent flutter. Another factor which requires investigation is built-in curvature of the panel in the streamwise or cross-stream direction.

LANGLEY AERONAUTICAL LABORATORY,
NATIONAL ADVISORY COMMITTEE FOR AERONAUTICS,
LANGLEY FIELD, VA., *April 20, 1955.*

# APPENDIX A

## SOLUTION BY MEANS OF LAPLACE TRANSFORMS

In a recent paper (ref. 6), a procedure is outlined for obtaining by means of Laplace transforms the exact solution for the flutter of a two-dimensional membrane which is subjected to a supersonic stream on one side and stagnant air on the other. This solution is called exact, inasmuch as the equation of motion for the system is solved directly without any limitation being imposed on the mode shape or frequency of flutter. Reference 6 also mentions that pure bending of a plate and the more general case in which plate bending and membrane stretching are combined could be treated in the same manner. The present report treats the latter case; namely, the flutter of a panel (plate) acted on by a middle-plane or axial force, such as tension, or compression less than the buckling load. In the body of the report this problem is solved by the generalized-coordinate approach, and the coordinates used are the normal modes of the panel with no axial force acting. In this appendix, for the sake of completeness, the solution to the same problem is derived by means of Laplace transforms to the point where numerical calculations can be made. The feasibility of applying the Laplace transform solution is examined, but no numerical results are obtained.

The integrodifferential equation to be solved is given by equation (2) which, upon substitution of the expression for $p(x,t)$ obtained from equations (5) to (9), may be written as

$$\frac{D}{c^4}Z''''-\omega^2 m_A Z-\frac{F}{c^2}Z''+\frac{\rho U^2}{c}\left\{\frac{1}{\beta}\left[i2k\int_0^x w_u(\xi)I_u(x-\xi)d\xi+\frac{d}{dx}\int_0^x w_u(\xi)I_u(x-\xi)d\xi\right]-\frac{i}{2}\frac{\rho_0}{\rho}\left[i2k\int_0^1 w_l(\xi)I_l(x-\xi)d\xi\right]\right\}=0 \tag{A1}$$

or alternatively as

$$\frac{D}{c^4}Z''''-\omega^2 m_A Z-\frac{F}{c^2}Z''+\frac{\rho U^2}{c}\left\{\frac{1}{\beta}\left[w_u(0)I_u(x)+\int_0^x I_u(x-\xi)\left(\frac{d}{d\xi}+i2k\right)w_u(\xi)d\xi\right]-\frac{i}{2}\frac{\rho_0}{\rho}\left[i2k\int_0^1 w_l(\xi)I_l(x-\xi)d\xi\right]\right\}=0 \tag{A2}$$

where

$$w_u(x)=Z'(x)+i2kZ(x)$$

$$w_l(x)=i2kZ(x)$$

$$I_u(x)=e^{-\overline{\omega}x}J_0\left(\frac{\overline{\omega}}{M}x\right)$$

$$I_l(x)=H_0^{(2)}(2k\overline{M}|x|)$$

Dividing equation (A2) by $m\omega^2$ yields

$$\alpha Z''''-\delta Z''-Z+\frac{1}{\mu}\frac{1}{4k^2}\left\{\frac{1}{\beta}\left[w_u(0)I_u(x)+\int_0^x I_u(x-\xi)\left(\frac{d}{d\xi}+i2k\right)w_u(\xi)d\xi\right]+\frac{-i}{2}\frac{\rho_0}{\rho}\left[i2k\int_0^1 w_l(\xi)I_l(x-\xi)d\xi\right]\right\}=0 \tag{A3}$$

where

$$\alpha=\frac{1}{K_1^4}\left(\frac{\omega_1}{\omega}\right)^2=\frac{1}{K_1^4}\Omega$$

$$\delta=\frac{F}{m_A c^2 \omega_1^2}\left(\frac{\omega_1}{\omega}\right)^2=f\Omega$$

The quantity $\omega_1$ in the formulas for $\alpha$ and $\delta$ is the first natural frequency of the plate vibrating in a vacuum with no axial force $F$ acting and $K_1$ is the associated eigenvalue. (See table I.) In the case of the membrane, $\omega_1$ would be the first natural frequency of the membrane, $\alpha$ would be zero ($D$ is negligible for the membrane), and $f$ would be $\left(\frac{1}{\pi}\right)^2$.

Applying the Laplace transform

$$L\{Z(x)\}=\overline{Z}(s)=\int_0^\infty e^{-sx}Z(x)dx$$

to equation (A3) (using in the process pairs 4 and 7, p. 294, ref. 17) yields the transformed problem in the form

$$\alpha(s^4\overline{Z}-s^3z_0-s^2z_1-sz_2-z_3)-\delta(s^2\overline{Z}-sz_0-z_1)-\overline{Z}+\frac{1}{4k^2\mu}\left(\frac{1}{\beta}[(s^2+i4ks-4k^2)\overline{Z}-(s+i2k)z_0]\,\overline{I}_u(s)+\frac{i}{2}\frac{\rho_0}{\rho}4k^2L\left\{\int_0^1 Z(\xi)I_1(x-\xi)d\xi\right\}\right)=0 \tag{A4}$$

where $z_0=Z(0)$, $z_1=Z'(0)$, $z_2=Z''(0)$, $z_3=Z'''(0)$, and $\overline{I}_u(s)$ is the Laplace transform of $I_u(x)$. The Laplace transform in equation (A4) involving $\rho_0/\rho$ as a multiplier is the contribution of the perturbation pressure on the lower surface of the panel. Unfortunately, this transform does not appear to be obtainable here where the deflection $Z$ is unknown. In the body of the report the effect of including the air below the panel is found to be moderate at a Mach number of 1.3 and reasons are given why this effect is expected to be even smaller at the higher Mach numbers investigated. In view of these facts and in view of the difficulty of handling the lower-surface term in equation (A4), this term will be omitted in the rest of this appendix—that is, treated as if $\rho_0$ were zero.

Equation (A4) can therefore be reduced to

$$[(\alpha s^4-\delta s^2-1)+\epsilon(s+i2k)^2\overline{I}_u(s)]\overline{Z}(s)=\alpha(s^2z_1+sz_2+z_3)-\delta z_1 \tag{A5}$$

where $\epsilon=1/4k^2\mu\beta$ and $z_0$ has been dropped because it is zero for the present boundary-value problems. Thus the integro-differential equation (A1) has been reduced to the algebraic equation (A5).

Now by means of pair 11, p. 294, and pair 55, p. 298, of reference 17 there is obtained

$$\overline{I}_u(s)=\left[(s+i\bar{\omega})^2+\left(\frac{\bar{\omega}}{M}\right)^2\right]^{-1/2} \tag{A6}$$

Therefore, from equation (A5), after some algebraic manipulation

$$\overline{Z}(s)=\frac{M(s)}{Q(s)}+\frac{N(s)}{Q(s)}\,\overline{I}_u(s) \tag{A7}$$

where

$$Q(s)=(\alpha s^4-\delta s^2-1)^2\left[(s+i\bar{\omega})^2+\left(\frac{\bar{\omega}}{M}\right)^2\right]-\epsilon^2(s+i2k)^4$$

$$M(s)=(\alpha s^4-\delta s^2-1)\left[(s+i\bar{\omega})^2+\left(\frac{\bar{\omega}}{M}\right)^2\right][\alpha(s^2z_1+sz_2+z_3)-\delta z_1]$$

$$N(s)=-\epsilon(s+i2k)^2\left[(s+i\bar{\omega})^2+\left(\frac{\bar{\omega}}{M}\right)^2\right][\alpha(s^2z_1+sz_2+z_3)-\delta z_1]$$

In polynomial form the quantities $Q$, $M$, and $N$ are

$$Q(s)=\sum_{r=0}^{10}q_r s^{10-r} \tag{A8}$$

$$M(s)=z_1\sum_{r=0}^{8}m_r^{(1)}s^{8-r}+z_2\sum_{r=0}^{7}m_r^{(2)}s^{7-r}+z_3\sum_{r=0}^{6}m_r^{(3)}s^{6-r} \tag{A9}$$

$$N(s)=z_1\sum_{r=0}^{6}n_r^{(1)}s^{6-r}+z_2\sum_{r=0}^{5}n_r^{(2)}s^{5-r}+z_3\sum_{r=0}^{4}n_r^{(3)}s^{4-r} \tag{A10}$$

The coefficients of the various series are given in the following table:

| $r$ | $q_r$ | $m_r^{(1)}$ | $m_r^{(2)}$ | $m_r^{(3)}$ | $n_r^{(1)}$ | $n_r^{(2)}$ | $n_r^{(3)}$ |
|---|---|---|---|---|---|---|---|
| 0 | $\alpha^2$ | $\alpha^2$ | $\alpha^2$ | $\alpha^2$ | $-\alpha\epsilon$ | $-\alpha\epsilon$ | $-\alpha\epsilon$ |
| 1 | $i2\bar{\omega}\alpha^2$ | $i2\bar{\omega}\alpha^2$ | $i2\bar{\omega}\alpha^2$ | $i2\bar{\omega}\alpha^2$ | $-i2\bar{\omega}\alpha\epsilon\left(1+\frac{\beta^2}{M^2}\right)$ | $-i2\bar{\omega}\alpha\epsilon\left(1+\frac{\beta^2}{M^2}\right)$ | $-i2\bar{\omega}\alpha\epsilon\left(1+\frac{\beta^2}{M^2}\right)$ |
| 2 | $-\left(2\alpha\delta+\alpha^2\frac{\beta^2\bar{\omega}^2}{M^2}\right)$ | $-\left(2\alpha\delta+\alpha^2\frac{\beta^2\bar{\omega}^2}{M^2}\right)$ | $-\left(\alpha\delta+\alpha^2\frac{\beta^2\bar{\omega}^2}{M^2}\right)$ | $-\left(\alpha\delta+\alpha^2\frac{\beta^2\bar{\omega}^2}{M^2}\right)$ | $\delta\epsilon+\alpha\epsilon\frac{\beta^2\bar{\omega}^2}{M^2}\left(5+\frac{\beta^2}{M^2}\right)$ | $\alpha\epsilon\frac{\beta^2\bar{\omega}^2}{M^2}\left(5+\frac{\beta^2}{M^2}\right)$ | $\alpha\epsilon\frac{\beta^2\bar{\omega}^2}{M^2}\left(5+\frac{\beta^2}{M^2}\right)$ |
| 3 | $-i4\bar{\omega}\alpha\delta$ | $-i4\bar{\omega}\alpha\delta$ | $-i2\bar{\omega}\alpha\delta$ | $-i2\bar{\omega}\alpha\delta$ | $i2\epsilon\left[\bar{\omega}\delta\left(1+\frac{\beta^2}{M^2}\right)+2\alpha\frac{\beta^4\bar{\omega}^2}{M^4}\right]$ | $i4\alpha\epsilon\frac{\beta^4\bar{\omega}^3}{M^4}$ | $i4\alpha\epsilon\frac{\beta^4\bar{\omega}^3}{M^4}$ |
| 4 | $\delta^2-2\alpha+\alpha\delta\frac{2\beta^2\bar{\omega}^2}{M^2}$ | $\delta^2-\alpha+2\alpha\delta\frac{\beta^2\bar{\omega}^2}{M^2}$ | $-\alpha+\alpha\delta\frac{\beta^2\bar{\omega}^2}{M^2}$ | $-\alpha+\alpha\delta\frac{\beta^2\bar{\omega}^2}{M^2}$ | $-\epsilon\frac{\beta^2\bar{\omega}^2}{M^2}\left[\alpha\frac{\beta^4\bar{\omega}^2}{M^4}+\delta\left(5+\frac{\beta^2}{M^2}\right)\right]$ | $-\alpha\epsilon\frac{\beta^6\bar{\omega}^4}{M^6}$ | $-\alpha\epsilon\frac{\beta^6\bar{\omega}^4}{M^6}$ |
| 5 | $i2\bar{\omega}(\delta^2-2\alpha)$ | $i2\bar{\omega}(\delta^2-\alpha)$ | $-i2\bar{\omega}\alpha$ | $-i2\bar{\omega}\alpha$ | $-i4\delta\epsilon\frac{\beta^4\bar{\omega}^3}{M^4}$ | 0 | |
| 6 | $2\delta-\epsilon^2-(\delta^2-2\alpha)\frac{\beta^2\bar{\omega}^2}{M^2}$ | $\delta-(\delta^2-\alpha)\frac{\beta^2\bar{\omega}^2}{M^2}$ | $\alpha\frac{\beta^2\bar{\omega}^2}{M^2}$ | $\alpha\frac{\beta^2\bar{\omega}^2}{M^2}$ | $\delta\epsilon\frac{\beta^6\bar{\omega}^4}{M^6}$ | | |
| 7 | $i(4\bar{\omega}\delta-8k^2\epsilon^2)$ | $i2\bar{\omega}\delta$ | 0 | | | | |
| 8 | $1-2\delta\frac{\beta^2\bar{\omega}^2}{M^2}+24k^2\epsilon^2$ | $-\delta\frac{\beta^2\bar{\omega}^2}{M^2}$ | | | | | |
| 9 | $i(2\bar{\omega}+32k^2\epsilon^2)$ | | | | | | |
| 10 | $-\left(\frac{\beta^2\bar{\omega}^2}{M^2}+16k^4\epsilon^2\right)$ | | | | | | |

The exact inverse transform of equation (A7) requires the determination of the roots of $Q(s)$ (eq. (A8)). Since $Q(s)$ is a tenth-order polynomial, its roots can be solved only approximately for specific values of the coefficients $q_r$. An alternative procedure is to expand the quantity $[Q(s)]^{-1}$ in a Maclaurin's series (a procedure used in ref. 18), with the result that it may be expressed in the form

$$\frac{1}{Q(s)}=\frac{1}{s^{10}}\sum_{n=0}^{\infty}\frac{T_n}{s^n} \tag{A11}$$

where

$$q_0T_0=1$$

$$q_0T_n=-\sum_{r=1}^{10}q_rT_{n-r} \qquad (n\geqq 1)$$

and $T$ with a negative subscript is to be interpreted as zero.

When the series expansion for $[Q(s)]^{-1}$ (eq. (A11)) is substituted into equation (A7), the transform $\overline{Z}(s)$ becomes the sum of infinite series with terms of the two distinct types

$$\frac{A}{s^m}$$

and

$$\frac{B}{s^m}\bar{I}_u(s)$$

where $m$ is a positive integer. The inverse Laplace transform of the first type of term is (see pair 3, p. 295 of ref. 17)

$$L^{-1}\left\{\frac{A}{s^m}\right\}=\frac{Ax^{m-1}}{(m-1)!} \tag{A12}$$

and of the second is (see pair 7, p. 294 of ref. 17)

$$L^{-1}\left\{\frac{B}{s^m}\bar{I}_u(s)\right\}=\frac{B}{(m-1)!}\int_0^x(x-\xi)^{m-1}I_u(\xi)d\xi \tag{A13}$$

where $I_u(x)$ is defined following equation (A2).

Upon substituting equations (A9), (A10), and (A11) into equation (A7) and using equations (A12) and (A13) to obtain the inverse transform of the resultant expression, $Z(x)$ is given by

$$Z(x)=h_1(x)z_1+h_2(x)z_2+h_3(x)z_3 \tag{A14}$$

where

$$h_1(x)=\sum_{n=0}^{\infty}\sum_{r=0}^{8}\frac{T_n m_r^{(1)}x^{n+r+1}}{(n+r+1)!}+\sum_{n=0}^{\infty}\sum_{r=0}^{6}\frac{T_n n_r^{(1)}}{(n+r+3)!}\int_0^x(x-\xi)^{n+r+3}I_u(\xi)d\xi$$

$$h_2(x)=\sum_{n=0}^{\infty}\sum_{r=0}^{7}\frac{T_n m_r^{(2)}x^{n+r+2}}{(n+r+2)!}+\sum_{n=0}^{\infty}\sum_{r=0}^{5}\frac{T_n n_r^{(2)}}{(n+r+4)!}\int_0^x(x-\xi)^{n+r+4}I_u(\xi)d\xi$$

$$h_3(x)=\sum_{n=0}^{\infty}\sum_{r=0}^{6}\frac{T_n m_r^{(3)}x^{n+r+3}}{(n+r+3)!}+\sum_{n=0}^{\infty}\sum_{r=0}^{4}\frac{T_n n_r^{(3)}}{(n+r+5)!}\int_0^x(x-\xi)^{n+r+5}I_u(\xi)d\xi$$

In deriving equation (A14) only one boundary condition—namely, $z_0=Z(0)=0$—has been used thus far. In order to obtain the solution for a plate restrained in a particular manner, it is necessary to impose three additional boundary conditions. These additional conditions for the plate with pinned and clamped edges are given in equations (3) and (4), respectively. By their use, one of the terms of equation (A14) is eliminated and two homogeneous equations in the two remaining unknown $z_i$'s are obtained. The borderline condition of harmonic oscillation, or the point at which flutter occurs, is obtained by setting the determinant of the coefficients of these equations equal to zero. Thus, the flutter determinant for the pinned-edge plate is

$$\begin{vmatrix} h_1(1) & h_3(1) \\ h_1''(1) & h_3''(1) \end{vmatrix}=0 \tag{A15}$$

and for the clamped-edge plate is

$$\begin{vmatrix} h_2(1) & h_3(1) \\ h_2'(1) & h_3'(1) \end{vmatrix}=0 \tag{A16}$$

where the determinant elements are given by

$$h_1(1)=\sum_{n=0}^{\infty}\sum_{r=0}^{8}\frac{T_n m_r^{(1)}}{(n+r+1)!}+\sum_{n=0}^{\infty}\sum_{r=0}^{6}\frac{T_n n_r^{(1)}}{(n+r+3)!}\int_0^1(1-\xi)^{n+r+3}I_u(\xi)d\xi$$

$$h_1''(1)=m_0^{(1)}\sum_{n=1}^{\infty}\frac{T_n}{(n-1)!}+\sum_{n=0}^{\infty}\sum_{r=1}^{8}\frac{T_n m_r^{(1)}}{(n+r-1)!}+\sum_{n=0}^{\infty}\sum_{r=0}^{6}\frac{T_n n_r^{(1)}}{(n+r+1)!}\int_0^1(1-\xi)^{n+r+1}I_u(\xi)d\xi$$

$$h_2(1)=\sum_{n=0}^{\infty}\sum_{r=0}^{7}\frac{T_n m_r^{(2)}}{(n+r+2)!}+\sum_{n=0}^{\infty}\sum_{r=0}^{5}\frac{T_n n_r^{(2)}}{(n+r+4)!}\int_0^1(1-\xi)^{n+r+4}I_u(\xi)d\xi$$

$$h_2'(1)=\sum_{n=0}^{\infty}\sum_{r=0}^{7}\frac{T_n m_r^{(2)}}{(n+r+1)!}+\sum_{n=0}^{\infty}\sum_{r=0}^{5}\frac{T_n n_r^{(2)}}{(n+r+3)!}\int_0^1(1-\xi)^{n+r+3}I_u(\xi)d\xi$$

$$h_3(1)=\sum_{n=0}^{\infty}\sum_{r=0}^{6}\frac{T_n m_r^{(3)}}{(n+r+3)!}+\sum_{n=0}^{\infty}\sum_{r=0}^{4}\frac{T_n n_r^{(3)}}{(n+r+5)!}\int_0^1(1-\xi)^{n+r+5}I_u(\xi)d\xi$$

$$h_3'(1)=\sum_{n=0}^{\infty}\sum_{r=0}^{6}\frac{T_n m_r^{(3)}}{(n+r+2)!}+\sum_{n=0}^{\infty}\sum_{r=0}^{4}\frac{T_n n_r^{(3)}}{(n+r+4)!}\int_0^1(1-\xi)^{n+r+4}I_u(\xi)d\xi$$

$$h_3''(1)=\sum_{n=0}^{\infty}\sum_{r=0}^{6}\frac{T_n m_r^{(3)}}{(n+r+1)!}+\sum_{n=0}^{\infty}\sum_{r=0}^{4}\frac{T_n n_r^{(3)}}{(n+r+3)!}\int_0^1(1-\xi)^{n+r+3}I_u(\xi)d\xi$$

Each of the preceding elements contains integrals of the form

$$I_m(M,\bar{\omega})=\int_0^1(1-\xi)^m I_u(\xi)d\xi \tag{A17}$$

which can be written in terms of the Schwarz functions $f_\lambda(M,\bar{\omega})$ (see ref. 9 or eq. (24)) as

$$I_m(M,\bar{\omega})=\sum_{\lambda=0}^{m}\frac{(-1)^\lambda m!}{(m-\lambda)!\lambda!}f_\lambda(M,\bar{\omega}) \tag{A18}$$

where

$$f_\lambda = \int_0^1 \xi^\lambda I_u(\xi) d\xi$$

Examination of the series in the elements of equations (A15) and (A16) reveals that $\lambda$ of equation (A18) ranges at least between 0 and $n+7$ and at most between 0 and $n+9$. In order to obtain accuracy to four significant figures, at least the first eight terms of each series and the consequent ranging of $\lambda$ between 0 and 16 are probably required. Inasmuch as the Schwarz functions $f_\lambda$ have been tabulated for only the first few values of $\lambda$, the use of equation (A18) would require the determination of a rather extensive series of $f_\lambda$'s. An alternative and perhaps more efficient procedure would be to evaluate directly the integrals $I_m$ as given in equation (A17) rather than to resort to the expanded form in equation (A18).

Attention will now be given to the solution of the determinantal equations (A15) and (A16). A method of solution for parameters that were sought in the generalized-coordinate approach of the body of the report (that is, $1/\mu$ and $2k_1=2k\ (R.P.\Omega)^{1/2}$) will be outlined here.

The elements of equations (A15) and (A16) are complex functions of the five parameters $M$, $k$, $\Omega$ (with $g=0$), $f$, and $1/\mu$. The most difficult parts of these elements to evaluate are the integrals generically represented by $I_m$ in equation (A17), which are functions of the parameters $M$ and $k$. Therefore, a convenient method of solution would be to fix the parameters $M$ and $k$ and preferably $f$ and vary the remaining parameters $\Omega$ and $1/\mu$ in the left-hand side (hereinafter referred to as $\Delta$) of equation (A15) or of equation (A16). By varying $\Omega$ and $1/\mu$ over sufficiently broad ranges, an indefinitely large number of combinations of $\Omega$ and $1/\mu$ which cause $\Delta$ to vanish could be found. Each combination would define a point on separate stability boundaries, such as those shown in figure 3. Each boundary could then be determined as completely as desired by varying $k$ over a sufficient range and repeating for each chosen value of $k$ the process of finding combinations of $\Omega$ and $1/\mu$ which cause $\Delta$ to vanish.

As can be surmised, the numerical calculations would be extremely lengthy even apart from two other questions which arise; namely, which is the stable side of each boundary, and has the critical boundary been found which separates stable and unstable regions and thereby defines the thinnest panel that is stable? In the present report, therefore, the stability boundaries shown in figures 2 to 9 were calculated exclusively on the basis of the generalized-coordinate or modal approach.

# APPENDIX B

## VELOCITY POTENTIAL $\phi_l$ AND RELATED INTEGRAL $\bar{\bar{P}}_n$

### VELOCITY POTENTIAL $\phi_l$

The velocity potential $\phi_l$ given in equation (9), which applies to the lower surface of the two-dimensional panel shown in figure 1, will now be derived. The system consists of a panel of width $c$, which is part of an otherwise rigid surface of infinite extent, oscillating harmonically with stationary air extending to infinity below. Thus, over the panel the normal velocity on the lower surface is $w_l=i\omega Z(x)e^{i\omega t}$, while over the rest of the plane $w_l=0$.

According to reference 10 the solution to this problem can be obtained from

$$\phi=-\frac{1}{2\pi}\iint w_l\frac{e^{-i\frac{\omega}{a}r}}{r}dS \tag{B1}$$

where $w_l$ is the given normal velocity at the element of area $dS$ of the plane and $\phi$ is the velocity potential at a point $P$ which is at a distance $r$ from $dS$. From equation (B1) the velocity potential at the surface of the panel may be obtained, in terms of the coordinates of figure 1, as

$$\phi_l=-\frac{i\omega e^{i\omega t}}{2\pi}\int_0^c Z(\xi)d\xi\int_{-\infty}^{\infty}\frac{e^{-i\frac{\omega}{a}\sqrt{(x-\xi)^2+y^2}}}{\sqrt{(x-\xi)^2+y^2}}dy \tag{B2}$$

Upon making the substitution $y=|x-\xi|\cosh\theta$, the integral with respect to $y$ in equation (B2) may be written in the form

$$I(x-\xi)=\int_{-\infty}^{\infty}\frac{e^{-i\frac{\omega}{a}\sqrt{(x-\xi)^2+y^2}}}{\sqrt{(x-\xi)^2+y^2}}dy=\int_{-\infty}^{\infty}e^{-i\frac{\omega}{a}|x-\xi|\cosh\theta}d\theta \tag{B3}$$

By means of equation (11) on page 180 of reference 19, equation (B3) becomes

$$I(x-\xi)=-i\pi H_0^{(2)}\left(\frac{\omega}{a}|x-\xi|\right) \tag{B4}$$

Substitution of equation (B4) into equation (B2) yields

$$\phi_l=-\frac{\omega e^{i\omega t}}{2}\int_0^c Z(\xi)H_0^{(2)}\left(\frac{\omega}{a}|x-\xi|\right)d\xi \tag{B5}$$

If the coordinates $x$ and $\xi$ are nondimensionalized by dividing by the panel chord $c$, the form for $\phi_l$ given in equation (9) is obtained.

### INTEGRAL $\bar{\bar{P}}_n$

The third term on the right-hand side of equation (22), namely,

$$\bar{\bar{P}}_n(x)=\frac{\rho_0}{\rho}\frac{1}{\pi}\int_0^1 Z_n(\xi)\log_e(kM|x-\xi|)d\xi \tag{B6}$$

contains the singularity of the Hankel function in equation (20).

As a first step in the evaluation of the improper integral in equation (B6), let

$$\left.\begin{aligned}\xi&=\frac{1}{2}(1-\cos\zeta)\\ x&=\frac{1}{2}(1-\cos\psi)\end{aligned}\right\} \tag{B7}$$

and

$$Z_n(\xi)=\sum_{m=1}^{\infty}S_m\sin m\zeta \tag{B8}$$

where

$$S_m=\frac{2}{\pi}\int_0^{\pi}Z_n(\zeta)\sin m\zeta\,d\zeta$$

In terms of equations (B7) and (B8), equation (B6) becomes

$$\bar{\bar{P}}_n(x)=\frac{\rho_0}{\rho}\frac{1}{2\pi}I(\psi) \tag{B9}$$

where

$$I(\psi)=\sum_{m=1}^{\infty}S_m\int_0^{\pi}\sin\zeta\sin m\zeta\log_e\left(\frac{kM}{2}|\cos\zeta-\cos\psi|\right)d\zeta \tag{B10}$$

Taking the derivative of equation (B10) with respect to $\psi$ and making use of reference 20 to evaluate the resulting improper integrals yields

$$\begin{aligned}\frac{dI}{d\psi}&=\frac{1}{2}\sum_{m=1}^{\infty}S_m\int_0^{\pi}\frac{\cos(m-1)\zeta-\cos(m+1)\zeta}{\cos\zeta-\cos\psi}\sin\psi\,d\zeta\\&=\frac{\pi}{2}\sum_{m=1}^{\infty}S_m[\sin(m-1)\psi-\sin(m+1)\psi]\end{aligned} \tag{B11}$$

Integration of equation (B11) gives

$$I(\psi)=\frac{\pi}{2}\left\{\frac{1}{2}S_1\cos2\psi+\sum_{m=2}^{\infty}S_m\left[\frac{\cos(m+1)\psi}{m+1}-\frac{\cos(m-1)\psi}{m-1}\right]\right\}+K \tag{B12}$$

The integration constant $K$ in equation (B12) is determined by setting $\psi$ equal to $\pi/2$ in equations (B10) and (B12) and equating the two resultant expressions. By so doing, it is found that

$$K=\frac{\pi}{2}S_1\log_e\frac{kM}{4} \tag{B13}$$

By means of equations (B12) and (B13), equation (B9) becomes

$$\begin{aligned}\bar{\bar{P}}_n(x)=\frac{\rho_0}{\rho}\frac{1}{4}\Bigg\{&\left(\log_e\frac{kM}{4}+\frac{1}{2}\cos2\psi\right)S_1+\\&\sum_{m=2}^{\infty}S_m\left[\frac{\cos(m+1)\psi}{m+1}-\frac{\cos(m-1)\psi}{m-1}\right]\Bigg\}\end{aligned} \tag{B14}$$

The mode shapes $Z_n$ in equation (B6) are now approximated by the finite sine series

$$Z_n(\xi) \approx \sum_{r=1}^{10} s_r \sin rx \tag{B15}$$

The constants $S_m$ in equation (B14) are obtained from the expression following equation (B8), with the result that equation (B14) can be written as

$$\overline{\overline{P}}_n(x) = \frac{\rho_0}{\rho} \frac{1}{4} \sum_{r=1}^{10} \overline{\overline{L}}_r(x) s_r \tag{B16}$$

where

$$\overline{\overline{L}}_1(x) = \log_e \frac{kM}{4} + \frac{1}{2} \cos 2\psi$$

$$\overline{\overline{L}}_r(x) = \frac{1}{r+1} \cos (r+1)\psi - \frac{1}{r-1} \cos (r-1)\psi \qquad (r \geq 2)$$

and, as in equation (B7),

$$x = \frac{1}{2}(1 - \cos \psi)$$

The form given in equation (B16) was used to obtain equation (28). Of interest is the fact that only $\overline{\overline{L}}_1$ depends on $k$ and $M$. The term $\overline{\overline{P}}_n$ is therefore comparatively simple to include in equation (22).

The coefficients $s_r$ in equations (B15) and (B16) for the first four modes of the plate with clamped edges are given in the following table:

| | Mode 1 | Mode 2 | Mode 3 | Mode 4 |
|---|---|---|---|---|
| $s_1$ | 0.66613 | 0 | −0.32917 | 0 |
| $s_2$ | 0 | 0.64119 | 0 | 0.40890 |
| $s_3$ | −0.29503 | 0 | −0.50867 | 0 |
| $s_4$ | 0 | −0.46861 | 0 | 0.27852 |
| $s_5$ | 0.039764 | 0 | 0.61134 | 0 |
| $s_6$ | 0 | 0.098515 | 0 | −0.61524 |
| $s_7$ | 0.001315 | 0 | −0.18746 | 0 |
| $s_8$ | 0 | −0.003411 | 0 | 0.25600 |
| $s_9$ | 0.000396 | 0 | 0.021697 | 0 |
| $s_{10}$ | 0 | 0.002858 | 0 | −0.028044 |

The coefficients $s_{10}$ for the second and fourth modes were obtained by forcing the slope of $Z_n$, as given by equation (B15), to be zero at $\psi=0$ (that is, at $x=0$). A similar table can be easily calculated for the pinned-edge plate.

## REFERENCES


1. Hayes, W.: A Buckled Plate in a Supersonic Stream. Rep. No. AL–1029, North American Aviation, Inc., May 10, 1950.
2. Miles, John W.: Dynamic Chordwise Stability at Supersonic Speeds. Rep. No. AL–1140, North American Aviation, Inc., Oct. 18, 1950.
3. Isaacs, R. P.: Transtability Flutter of Supersonic Aircraft Panels. U. S. Air Force Project RAND P–101, The Rand Corp., July 1, 1949.
4. Fung, Y. C.: The Static Stability of a Two-Dimensional Curved Panel in a Supersonic Flow, With an Application to Panel Flutter. Jour. Aero. Sci., vol. 21, no. 8, Aug. 1954, pp. 556–565.
5. Shen, S. F.: Flutter of a Two-Dimensional Simply-Supported Uniform Panel in a Supersonic Stream. Contract No. N5ori-07833, Office of Naval Res.. Dept. Aero. Eng., M.I.T., Aug. 6, 1952.
6. Goland, Martin, and Luke, Yudell L.: An Exact Solution for Two-Dimensional Linear Panel Flutter at Supersonic Speeds. Jour. Aero. Sci. (Readers' Forum), vol. 21, no. 4, Apr. 1954, pp. 275–276.
7. Hedgepeth, John M., Budiansky, Bernard, and Leonard, Robert W.: Analysis of Flutter in Compressible Flow of a Panel on Many Supports. Jour. Aero. Sci., vol. 21, no. 7, July 1954, pp. 475–486.
8. Reissner, Eric, and Stein, Manuel: Torsion and Transverse Bending of Cantilever Plates. NACA TN 2369, 1951.
9. Garrick, I. E., and Rubinow, S. I.: Flutter and Oscillating Air-Force Calculations for an Airfoil in a Two-Dimensional Supersonic Flow. NACA Rep. 846, 1946. (Supersedes NACA TN 1158.)
10. Rayleigh, (Lord): The Theory of Sound. First American ed., vol. II, sec. 302, Dover Publications, 1945, p. 162.
11. Duncan, W. J.: Galerkin's Method in Mechanics and Differential Equations. R. & M. No. 1798, British A.R.C., 1937.
12. Theodorsen, Theodore, and Garrick, I. E.: Mechanism of Flutter—A Theoretical and Experimental Investigation of the Flutter Problem. NACA Rep. 685, 1940.
13. Scanlan, Robert H., and Rosenbaum, Robert: Introduction to the Study of Aircraft Vibration and Flutter. The Macmillan Co., 1951.
14. Dugundji, John: A Nyquist Approach to Flutter. Jour. Aero. Sci. (Readers' Forum), vol. 19, no. 6, June 1952, pp. 422–423.
15. Morse, Philip M.: Vibration and Sound. Second ed., McGraw-Hill Book Co., Inc., 1948.
16. Sylvester, Maurice A., and Baker, John E.: Some Experimental Studies of Panel Flutter at Mach Number 1.3. NACA RM L52I16, 1952.
17. Churchill, Ruel V.: Modern Operational Mathematics in Engineering. McGraw-Hill Book Co., Inc., 1944.
18. Runyan, Harry L., and Watkins, Charles E.: Flutter of a Uniform Wing With an Arbitrarily Placed Mass According to a Differential-Equation Analysis and a Comparison With Experiment. NACA Rep. 966, 1950. (Supersedes NACA TN 1848.)
19. Watson, G. N.: A Treatise on the Theory of Bessel Functions. Second ed., The Macmillan Co., 1944.
20. Glauert, H.: The Elements of Aerofoil and Airscrew Theory. Second ed., Cambridge Univ. Press, 1947 (Reprinted 1948), pp. 92–93.